The Plant Cell, Vol. 19: 1930–1946, June 2007, www.plantcell.org © 2007 American Society of Plant Biologists

ACTIN BINDING PROTEIN29 from *Lilium* Pollen Plays an Important Role in Dynamic Actin Remodeling [W][OA]

Yun Xiang,[a] Xi Huang,[a] Ting Wang,[a] Yan Zhang,[a] Qinwen Liu,[a] Patrick J. Hussey,[b] and Haiyun Ren[a,1]

[a] Key Laboratory of Cell Proliferation and Regulation Biology of Ministry of Education and College of Life Science, Beijing Normal University, Beijing 100875, People's Republic of China

[b] Integrative Cell Biology Laboratory, School of Biological and Biomedical Sciences, University of Durham, Science Laboratories, Durham DH1 3LE, United Kingdom

Villin/gelsolin/fragmin superfamily proteins have been shown to function in tip-growing plant cells. However, genes encoding gelsolin/fragmin do not exist in the *Arabidopsis thaliana* and rice (*Oryza sativa*) databases, and it is possible that these proteins are encoded by villin mRNA splicing variants. We cloned a 1006-bp full-length cDNA from *Lilium longiflorum* that encodes a 263–amino acid predicted protein sharing 100% identity with the N terminus of 135-ABP (*Lilium* villin) except for six C-terminal amino acids. The deduced 29-kD protein, *Lilium* ACTIN BINDING PROTEIN29 (ABP29), contains only the G1 and G2 domains and is the smallest identified member of the villin/gelsolin/fragmin superfamily. The purified recombinant ABP29 accelerates actin nucleation, blocks barbed ends, and severs actin filaments in a Ca^{2+}- and/or phosphatidylinositol 4,5-bisphosphate–regulated manner in vitro. Microinjection of the protein into stamen hair cells disrupted transvacuolar strands whose backbone is mainly actin filament bundles. Transient expression of ABP29 by microprojectile bombardment of lily pollen resulted in actin filament fragmentation and inhibited pollen germination and tube growth. Our results suggest that ABP29 is a splicing variant of *Lilium* villin and a member of the villin/gelsolin/fragmin superfamily, which plays important roles in rearrangement of the actin cytoskeleton during pollen germination and tube growth.

INTRODUCTION

The actin cytoskeleton is present in all eukaryotic cells and has crucial functions in many cellular processes. The highly dynamic feature of the actin cytoskeleton during polymerization, depolymerization, and rearrangements of actin polymers is the key for these diverse functions. The dynamic nature of the actin cytoskeleton is directly determined spatially and temporally by the actions of numerous actin binding proteins (ABPs) whose spatiotemporal activities are in turn under the control of a variety of parameters, such as Ca^{2+}, pH, phosphorylation, phosphoinositides, etc. (Franklin-Tong, 1999; Hepler et al., 2001; Monteiro et al., 2005; Hussey et al., 2006). The activity of different classes of ABPs regulates aspects of actin biochemistry, including nucleation, bundling, filament capping, fragmentation, and monomer availability. Several of these classes have been identified and are well characterized in pollen tubes, which is an ideal model system for studying the plant actin cytoskeleton and the molecular mechanisms regulating actin filament dynamics and spatial distribution. Among these proteins is the villin/gelsolin/fragmin superfamily. These are the only known Ca^{2+}-dependent actin binding proteins, and they seem to regulate actin remodeling and bundle formation within the Ca^{2+} gradients of the tip-growing pollen tubes.

The villin/gelsolin/fragmin superfamily proteins are ABPs, which are typified by the possession of three or six gelsolin-like domains that display internal homology with each other. The mammalian gelsolin, a single gene encoding an 82- to 84-kD protein containing six gelsolin-like domains (Vandekerckhove, 1990; Burtnick et al., 1997), is the founding member of the family. It nucleates, binds, severs, and caps actin filaments in a Ca^{2+}-dependent manner. The typical villin has six gelsolin-like domains and an additional small (8.5-kD) C-terminal domain called the headpiece, which is the main difference compared with gelsolin. The villin core retains the Ca^{2+}-dependent actin-severing, -capping, and -nucleating functions of villin, whereas the headpiece endows villin with the ability to form microfilament bundles (Friederich et al., 1990; Hartwig and Kwiatkowski, 1991). Proteins comprising three gelsolin-like domains, like severin from *Dictyostelium* (Yamamoto et al., 1982), fragmin from *Physarum* (Furuhashi and Hatano, 1989), and CapG from vertebrates, are F-actin capping and/or severing factors. These are encoded by distinct genes. The first plant homolog of villin to be described was isolated from lily (*Lilium*) pollen (Yokota et al., 1998). This plant villin can bind and bundle F-actin in vivo (Tominaga et al., 2000) and generate F-actin bundles of uniform polarity in vitro in a calcium-dependent fashion (Yokota et al., 1998; Yokota and Shimmen, 1999), although not all plant villins are calcium-dependent (Huang et al., 2005). The *Arabidopsis* genome contains five villin genes. Each of these genes is expressed in a wide range of tissues (Klahre et al., 2000; Staiger and Hussey, 2004). This is in contrast with the expression

[1] To whom correspondence should be addressed. E-mail hren@bnu.edu.cn; fax 86-10-58807721.
The author responsible for distribution of materials integral to the findings presented in this article in accordance with the policy described in the Instructions for Authors (www.plantcell.org) is: Haiyun Ren (hren@bnu.edu.cn).
[W]Online version contains Web-only data.
[OA]Open Access articles can be viewed online without a subscription.
www.plantcell.org/cgi/doi/10.1105/tpc.106.048413

pattern of mammalian villin, which is restricted to the microvilli of brush border cells. Plant villin is involved in organizing the cytoplasm in root hairs. Injection of antibodies against villin resulted in disintegration of the actin filament bundles, followed by the disappearance of transvacuolar strands (Tominaga et al., 2000), demonstrating that villin is an essential component of the actin filament bundle structure in tip-growing plant cells. However, studies of the smaller members of this superfamily are limited. Gelsolin-like proteins have been identified by immunoblotting in maize (*Zea mays*) and *Lilium longiflorum* pollen (Wu and Yan, 1997; Tao and Ren, 2003). Recently, a gelsolin-like 80-kD protein from *Papaver rhoeas* (poppy) pollen (Pr ABP80) was isolated and characterized biochemically (Huang et al., 2004). Poppy gelsolin shows Ca^{2+}-regulated actin filament–severing and barbed end–capping activities. This protein has been proposed to play a central role during the Ca^{2+}-mediated depolymerization of actin during self-incompatibility response in *P. rhoeas* pollen. A fragmin-like protein has also been identified from *Mimosa pudica* (Yamashiro et al., 2001) and *Lilium davidii* (Fan et al., 2004) pollen. Characterization of the fragmin-like protein (Ld ABP41) from *L. davidii* pollen shows that Ld ABP41 belongs to the gelsolin superfamily and functions in pollen tube growth (Fan et al., 2004). However, bioinformatic analysis shows that separate genes for gelsolin/fragmin do not exist in the *Arabidopsis thaliana* and rice (*Oryza sativa*) genome databases. Although it is possible that these proteins are encoded by mRNA splicing variants of villins, no direct evidence has been provided.

Here, we show that a full-length cDNA encoding a 29-kD protein (ACTIN BINDING PROTEIN29 [ABP29]) is expressed in *L. longiflorum* pollen, and sequence analysis of genomic and cDNA clones suggests that ABP29 is a splicing variant of the 135-ABP gene (*Lilium* villin). In vitro activity and in vivo function analyses reveal that ABP29 retains the activities of a typical member of the villin/gelsolin/fragmin superfamily, although it lacks the G3 domain that exists in all previously identified members, and that ABP29 may participate in regulating the rearrangement of the actin cytoskeleton during pollen germination and tube growth.

RESULTS

Isolating a Full-Length cDNA Encoding a Member of the Villin/Gelsolin/Fragmin Superfamily

To identify new members of the villin/gelsolin/fragmin superfamily that share internal homology with each other, nested PCR was used and succeeded in isolating a 1006-bp full-length cDNA sequence that contains a 792-bp coding region, a 5′ untranslated region (UTR; 111 bp), a 3′ UTR (103 bp), and a poly(A) tail from a *L. longiflorum* pollen cDNA expression library. The identical sequence was also obtained by RT-PCR from *L. longiflorum* pollen RNA. Sequencing analysis indicates that the cDNA sequence is exactly the same as that of 135-ABP (a *Lilium* villin) (Vidali et al., 1999) except for the last 16 bp before the stop codon TAA and the entire 3′ UTR. The cDNA encodes a protein of 263 amino acids with a molecular mass of 29 kD. Because the predicted protein shares high identity with the N-terminal sequences of villin/gelsolin/fragmin superfamily members of other species (Figure 1), it is assumed that the protein is a new member of the villin/gelsolin/fragmin superfamily. Hereafter, the protein is called ABP29. ABP29 only contains the G1, G2, and part of the G2-G3 linker sequence and differs from all known members of the villin/gelsolin/fragmin family.

We tested the possibility that ABP29 and 135-ABP were encoded by the same gene. A partial genomic sequence of 763 bp from the *L. longiflorum* genome was amplified by PCR using oligonucleotides generated to the sequence shared by the ABP29 and the 135-ABP cDNA for the forward primer and to the specific 3′ UTR of ABP29 for the reverse primer. A comparison of the partial genomic sequence with cDNAs for ABP29 and 135-ABP indicated that the genomic sequence contained two introns and a fragment unique to the ABP29 cDNA (Figure 2). The specific fragment that contains the 16-bp sequence starting with GT and the 3′ UTR of the ABP29 cDNA is apparently derived from part of the third intron of the gene encoding 135-ABP, because GT at acceptor (5′) splice sites is a conserved sequence for the majority of introns (Kalyna et al., 2006). In addition, the 5′ leader sequence and the coding sequence for the ABP29 and 135-ABP cDNAs are identical up to the 5′ GT of the possible third intron in 135-ABP (Figure 2). An identical clone was also identified in *Lilium siberia*. Because genes solely encoding gelsolin/fragmin do not exist in either the *Arabidopsis* or rice genome database, we conclude that the cDNA encoding ABP29 is a splicing product of a pre-ended transcription from 135-ABP.

The villin/gelsolin/fragmin superfamily members share a high degree of amino acid sequence identity in the N-terminal half of the proteins; therefore, the x-ray crystal structures of EGTA-gelsolin and the N-terminal halves of gelsolin (Burtnick et al., 1997, 2004; Robinson et al., 1999; Choe et al., 2002) were used as a template for modeling the overall structure and the Ca^{2+} and phosphatidylinositol 4,5-bisphosphate (PIP_2) binding sites of ABP29 (Figures 1 and 3). Gelsolin possesses two classes of Ca^{2+} binding sites. Type I sites are shared between Glu-167 on actin and gelsolin G-actin binding domains (G1 and G4), characterized by the coordination between a conserved Asp from the C-terminal end of an H1 helix and carbonyl oxygen atoms five and seven residues farther along the polypeptide. Type II sites are contained within gelsolin, which is characterized by a conserved Glu as the third residue in the H1 helix, a conserved Asp one residue prior to the C strand, and a carbonyl oxygen atom from the residue prior to the Asp (Choe et al., 2002). Similarly, there are three conserved Ca^{2+} binding sites identified in ABP29: type I in G1 (IG1), the Ca^{2+} binding residues Asp-89, Gly-94, and Ala-96 from G1 and Glu-167 from actin; type II in G1 (IIG1), the Ca^{2+} binding residues Gly-45, Asp-46, and Glu-77 from G1 and Val-125 on the G1-G2 linker; and Type II in G2 (IIG2), the Ca^{2+} binding residues Asp-165, Asp-166, and Glu-188 from G2 (Figure 3). Gelsolin has two PIP_2 binding sites in the linker between G1 and G2 (Yu et al., 1992), whereas ABP29 has only one conserved PIP_2 binding site (140 to 148). Structurally, ABP29 is a characteristic Ca^{2+}- and PIP_2-regulated actin binding protein. Because of the absence of the G3 domain that exists in all other members of the villin/gelsolin/fragmin superfamily, the biochemical properties and function of ABP29 were further tested in vitro and in vivo, as described below.

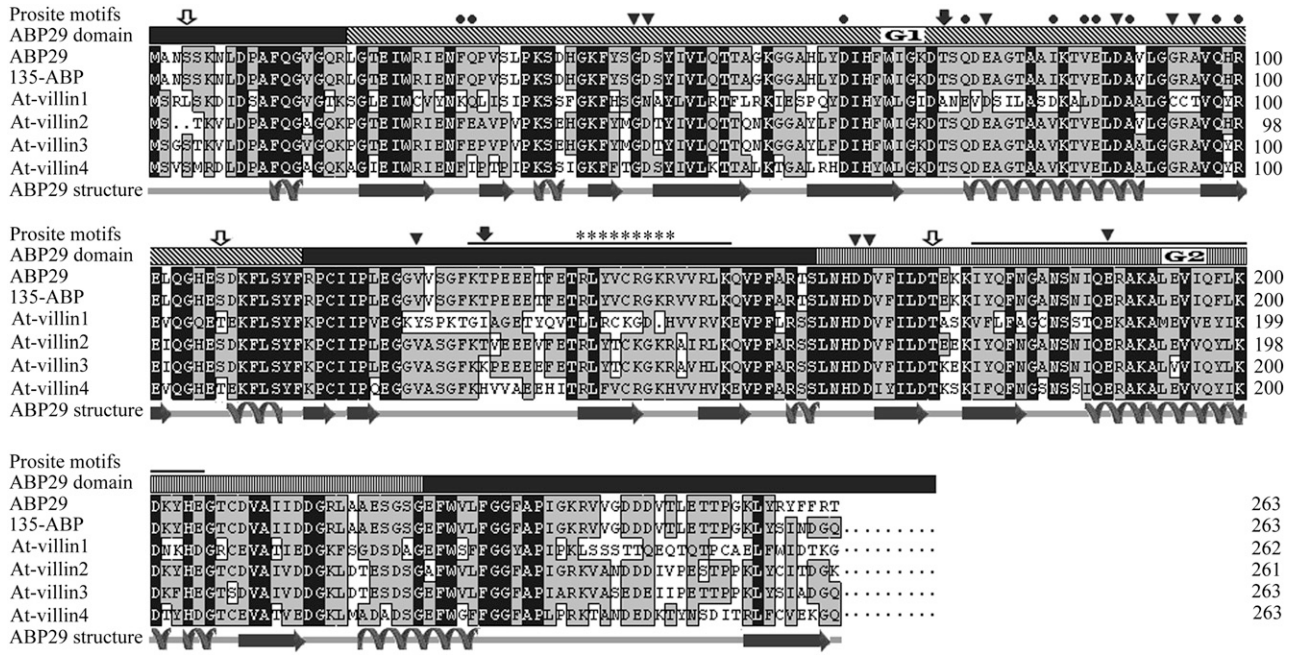

Figure 1. Multiple Alignment and Analysis of Amino Acid Sequences of Several Members of the Villin/Gelsolin/Fragmin Superfamily.

The secondary structural elements of the core region of ABP29 were predicted by Predict Protein Server (http://bubic.bioc.columbia.edu/pp/), and the amino acid sequence alignment of the 135-ABP, At villin1, At villin2, At villin3, and At villin4 was performed by DNAMAN software (prediction accuracy = 69.69%). The ABP29 domains are depicted by different symbols: G1 (19 to 114), an overhead bar with diagonal stripes marked with G1; G2 (162 to 225), an overhead bar with thin stripes marked with G2. The three thick solid lines above the sequence indicate the segment prior to G1, the G1-G2 linker (115 to 161), and the G2-G3 linker (226 to 263), respectively. Broad arrows and revolving lines under the sequences denote β-sheets and α-helices, respectively. Possible phosphorylation sites were obtained with PROSITE motif search: protein kinase C is marked by open arrows, and casein kinase II is marked by closed arrows. A possible PIP_2 binding region is represented by asterisks, and important Ca^{2+} binding residues are indicated by triangles above the sequences; G-actin binding residues are marked by closed circles, and F-actin binding residues are marked by thin lines. Letters in black blocks indicate 100% homology between these sequences, and those in gray blocks indicate ⩾50% homology.

Identification of ABP29 in Lily Total Pollen Extracts and Generation of Recombinant ABP29

A slightly modified procedure for purifying Ld ABP41 (a fragmin-like protein from *L. davidii*) by affinity chromatography on DNase I–Sepharose was used to identify the presence of ABP29 in lily pollen and the Ca^{2+}-dependent binding activity of ABP29 to monomeric actin (Fan et al., 2004). The crude protein extract from lily pollen was passed through a DNase I column, and the column was washed with a one-fourth volume of Ca^{2+} buffer as described previously for the purification of Ld ABP41 (Fan et al., 2004) to remove proteins nonspecifically bound to G-actin. Proteins bound to actin in a Ca^{2+}-dependent manner were ultimately eluted with an EGTA buffer. Bands at ~41 and 29 kD were observed (Figure 4A, lane 1), and both of them were recognized by affinity-purified anti-Ld ABP41 antibodies (Figure 4A, lane 3), indicating that these proteins might share homology. However, the amount of 29-kD protein was approximately one-tenth that of the 41-kD protein. The 41-kD polypeptide is the Ld ABP41 previously reported by our group (Fan et al., 2004), and the 29-kD polypeptide is consistent with the predicted molecular mass of ABP29. These results suggest that ABP29 is present in lily pollen and that it has Ca^{2+}-dependent monomeric actin binding activity.

To confirm that ABP29 is not a degradation product from the villin/gelsolin/framin superfamily proteins in lily pollen, the dynamic expression patterns of the superfamily proteins were compared by subjecting the lily pollen total proteins from different pollen tube development phases to protein gel blot analysis. As shown in Supplemental Figure 1A online, the purified anti-Ld ABP41 antibody recognized the 29-, 41-, 80-, 115-, and 135-kD protein bands from dehydrated, hydrated, or germinating lily pollen grains, which should correspond to ABP29, Ld ABP41 (Fan et al., 2004), ABP80 (Huang et al., 2004), 115-ABP (Nakayasu et al., 1998; Yokota et al., 2003), and 135-ABP (Yokota et al., 1998), respectively. Optical density analysis showed that during pollen tube development, the amount of Ld ABP41 decreases dramatically to one-tenth and ABP80 increases approximately three times (see Supplemental Figure 1B online); 115-ABP and 135-ABP merely turn up in the pollen germination, but ABP29 levels remain almost constant. This assay provided us with the evidence that ABP29 is not a degradation product from Ld ABP41 or villins.

To characterize the functional properties of ABP29 in vitro and in vivo, recombinant glutathione *S*-transferase (GST)–ABP29 was expressed in *Escherichia coli* and affinity-purified to >90% purity (Figure 4B, lane 1). The protein was recognized by the purified anti-Ld ABP41 antibodies (Figure 4B, lane 2). The GST-tagged

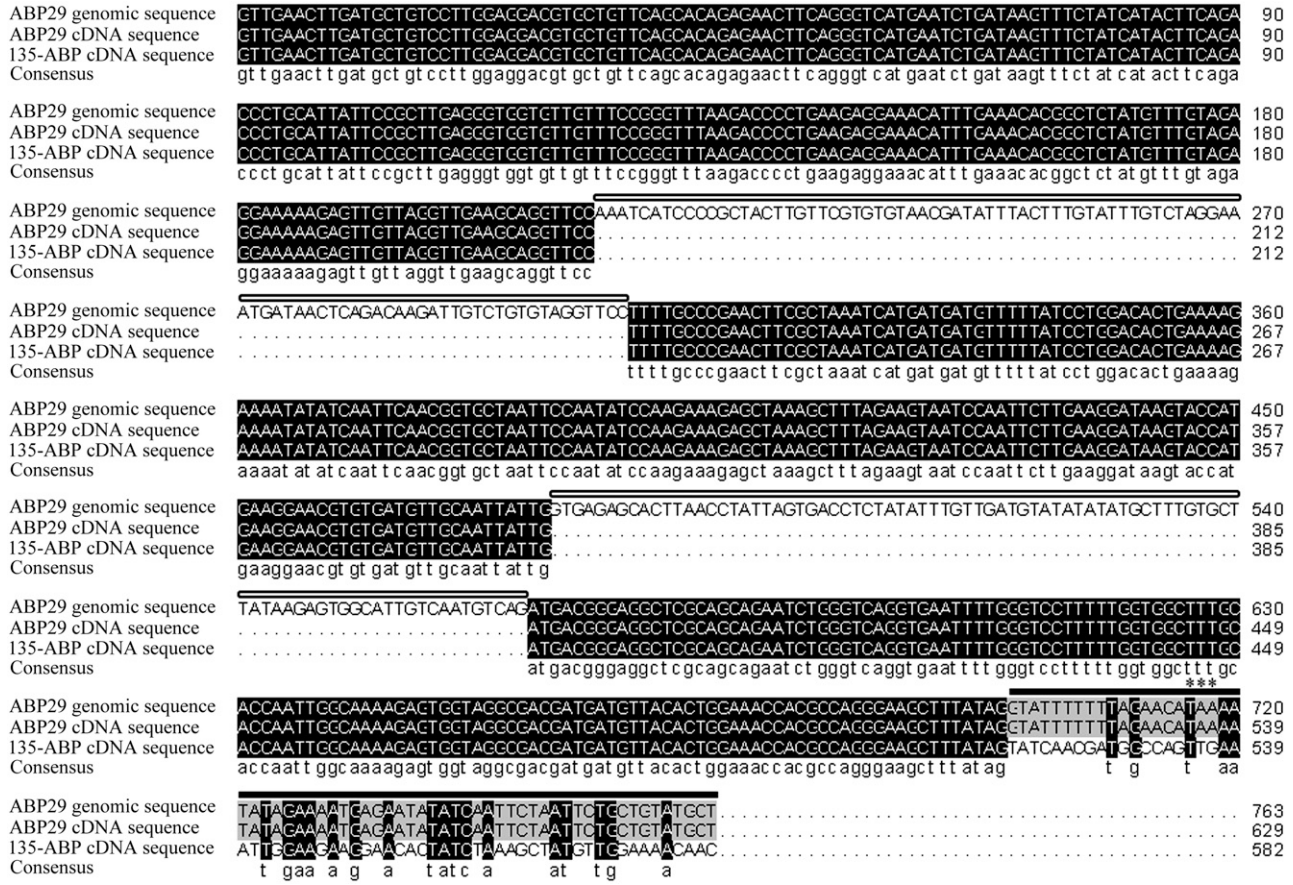

Figure 2. Multiple Alignment and Analysis of Sequences with Partial Genomic Sequence of ABP29, cDNA Sequences of ABP29, and 135-ABP.

Comparison of the ABP29 partial genomic sequence, cDNA sequences of ABP29, and 135-ABP was performed by DNAMAN software. The black blocks indicate 100% homology among these sequences, and the gray blocks indicate ≥50% homology. The two fragments of ABP29 partial genomic sequence (shown by open frames above the sequences) are absent in cDNA sequences of ABP29 and 135-ABP, which are deduced to be two introns of the gene encoding ABP29 and 135-ABP. The 3′ end specific sequence in cDNA of ABP29 (shown by a black frame above the sequences) is identical with that of the ABP29 genomic sequence and different from the cDNA sequence of 135-ABP, which is assumed to be an intron of the gene encoding 135-ABP. The stop codon of the ABP29 gene is denoted by asterisks.

ABP29 was used for the bulk of our studies that concern the role of ABP29 in actin-nucleating, -severing, and -capping activities.

ABP29 Binds to and Severs Actin Filaments in a Ca^{2+}-Sensitive Manner

The interaction of ABP29 with F-actin was determined with a high-speed cosedimentation assay. As shown in Figure 5A, nearly all of the prepared F-actin was sedimented at 200,000*g* in the absence of ABP29 with or without Ca^{2+} (Figure 5A, lanes 3 and 4), and the ABP29 was mostly soluble (Figure 5A, lanes 1 and 2). However, a significant amount of ABP29 sedimented with F-actin in the presence of 200 μM Ca^{2+} (Figure 5A, lanes 5 to 10), indicating that ABP29 binds to F-actin. Yet, in the presence of 2 mM EGTA, a little ABP29 sedimenting with F-actin was detected (Figure 5A, lanes 5 to 10), indicating that the F-actin binding activity of ABP29 is Ca^{2+}-dependent. In addition, the presence of ABP29 resulted in a redistribution of a significant amount of G-actin in the supernatant, suggesting that ABP29 severs or depolymerizes actin filaments. As shown in Figure 5B, when 5 μM actin was polymerized in the presence of 0.4, 0.8, or 1.6 μM ABP29 and 200 μM Ca^{2+}, the percentage of actin in the supernatant was 21.75% ± 3.15%, 25.42% ± 3.05%, and 32.04% ± 2.35% ($n = 4$), respectively, which is significantly higher than that of the control (5.03% ± 0.48%). However, in the presence of various concentrations of ABP29 and 2 mM EGTA, the percentage of actin in the supernatant was reduced sharply to 5.50% ± 1.10%, 6.38% ± 0.68%, and 6.25% ± 1.69% ($n = 4$), respectively, which is not significant compared with the control (5.37% ± 0.45%). These data indicate that ABP29 can bind and sever or depolymerize F-actin in a Ca^{2+}-dependent manner.

The severing activity of ABP29 was observed directly with the fluorescence microscope to test whether the ABP29 can sever Alexa 488–phalloidin-labeled prepolymerized F-actin. As shown in Figure 5C, 100 nM ABP29 significantly reduced the length of actin filaments (average mean = 1.8 ± 0.4 μm; $n = 200$) after

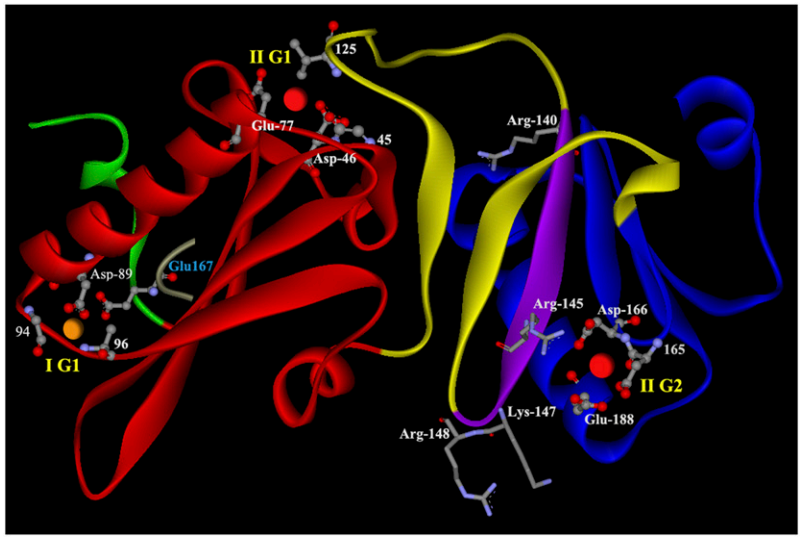

Figure 3. Predicted Structure, Conserved Ca^{2+}, and PIP_2 Binding Residues of ABP29 in the Absence of Ca^{2+}.

Predicted structural model of the ABP29 G1-G2 segment (residues 7 to 226) produced by the Swiss-Model program (http://www.expasy.ch/) and then colored with DS Visualizer software (version 1.5; Accelrys). The ABP29 domains are depicted by different colors: the segment prior to G1 (1 to 18), green; G1 (19 to 114), red; the G1-G2 linker (115 to 161), yellow; G2 (162 to 225), blue. Three Ca^{2+} binding sites characterized by the conserved calcium ion binding sites of the villin/gelsolin family are found in ABP29. Type I Ca^{2+} binding site is labeled (I) and shown as an orange sphere; type II Ca^{2+} binding sites are labeled (II) and shown as red spheres. The whole Ca^{2+} binding sites are labeled by balls and sticks. The PIP_2 binding residues (140 to 148) are colored purple, and the conserved protein residues in the RXXXXRXKR motif (underlined) are labeled by sticks. IG1 is coordinated by Glu-167 (blue letters) of actin (cyan).

incubation in the presence of 200 μM free Ca^{2+} for 30 min compared with the control (average mean = 9.21 ± 1.63 μm). When incubated with 100 nM ABP29 and 2 mM EGTA, the length of actin filaments was largely restored (average mean = 5.86 ± 1.01 μm), indicating that the severing activity of ABP29 is Ca^{2+}-dependent. PIP_2 plays a pivotal role in the phosphoinositide cycle that drives signaling, cytoskeletal organization, and membrane trafficking. Numerous cytoskeletal proteins, including gelsolin, are affected by PIP_2 in vitro (Sun et al., 1999). Therefore, a similar experiment was performed to examine the effect of PIP_2 on the severing activity of ABP29 in the presence of 200 μM Ca^{2+}. In the presence of 5 μM PIP_2, the length of the actin filaments was longer (average mean = 6.31 ± 0.92 μm) than that in the absence of PIP_2, demonstrating that the severing function of ABP29 is also PIP_2-sensitive.

To further observe the live severing process of actin filaments by ABP29, the time course of actin filament length reduction was recorded with a fluorescence microscope equipped with a CCD camera. As shown in Figure 5D, individual filaments showed an increasing number of breaks (arrowheads) as time elapsed, which was consistent with the severing activity of ABP29 (Figure 5C).

ABP29 Has Ca^{2+}-Dependent Nucleation Activity

To examine the effect of ABP29 on the dynamics of actin polymerization, pyrene fluorescence was used to monitor rabbit muscle actin polymerization kinetics. ABP29 at different concentrations was incubated for 5 min with 5 μM actin (5% pyrene-labeled) in the presence of 200 μM free Ca^{2+}. ABP29 eliminated the lag period of actin assembly from monomers and nucleated filament formation in a dose-dependent manner (Figure 6A). Similar experiments were performed to test whether the nucleating activity of ABP29 is Ca^{2+}-dependent. EGTA at various concentrations was applied to provide different concentrations of

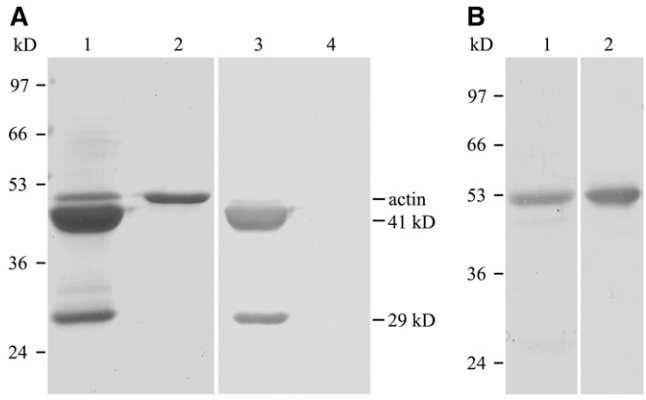

Figure 4. Identification of ABP29 from Lily Total Pollen Proteins and Purification of Recombinant ABP29 from *E. coli*.

(A) Coomassie blue–stained gel of lily pollen protein purified by affinity chromatography using DNase I–Sepharose (lane 1); lily pollen actin is the negative control (lane 2); protein gel blot of the purified proteins (lane 3) and actin (lane 4) probed with affinity-purified anti-Ld ABP41 antibody.
(B) Coomassie blue–stained gel of purified recombinant ABP29 (lane 1); protein gel blot of recombinant ABP29 (lane 2) probed with affinity-purified anti-Ld ABP41 antibody.

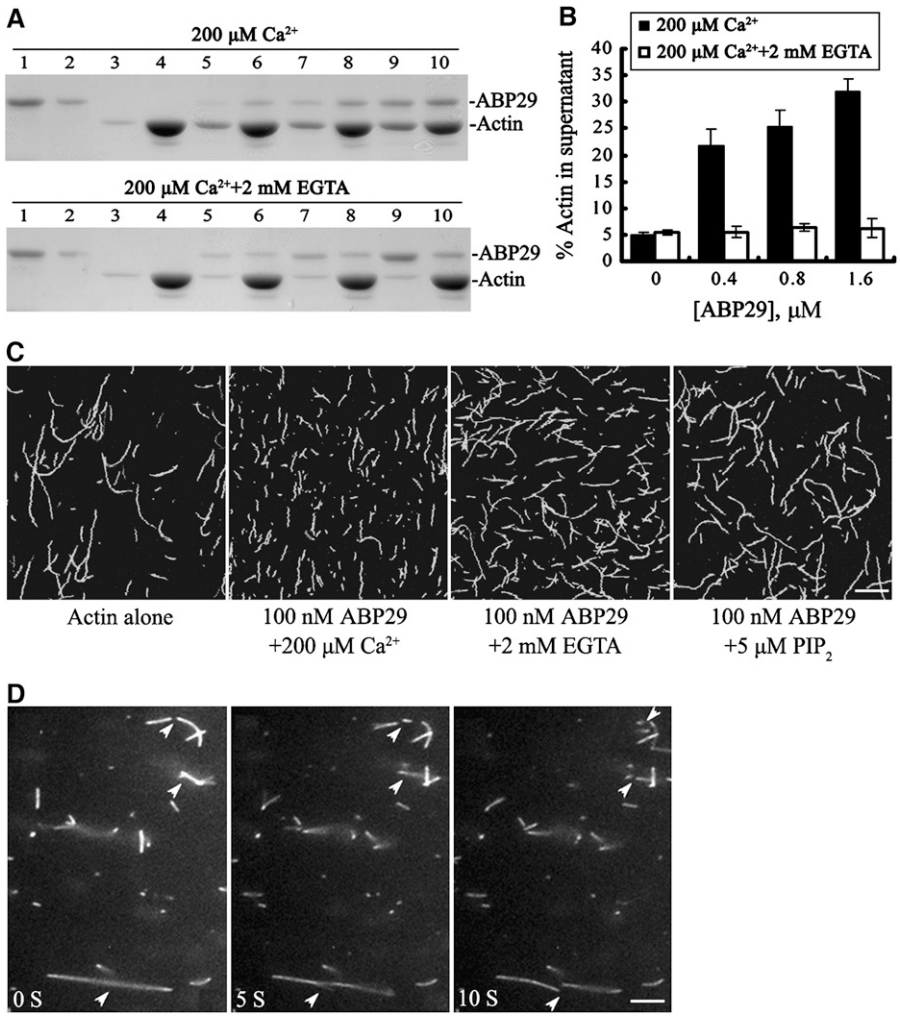

Figure 5. ABP29 Binds and Severs Actin Filaments in a Ca^{2+}- and PIP_2-Regulated Manner.

(A) A high-speed cosedimentation assay was used to determine ABP29's F-actin binding and severing functions. Mixtures of ABP29 at different concentrations and 5 μM preformed F-actin were centrifuged at 200,000*g* for 1 h at 4°C. The resulting supernatants and pellets were subjected to SDS-PAGE and stained with Coomassie blue. Lanes 1 and 2, ABP29 alone in the supernatant and pellet, respectively; lanes 3 and 4, actin alone in the supernatant and pellet, respectively; lanes 5 and 6, actin in the presence of 0.4 μM ABP29 in the supernatant and pellet, respectively; lanes 7 and 8, actin in the presence of 0.8 μM ABP29 in the supernatant and pellet, respectively; lanes 9 and 10, actin in the presence of 1.6 μM ABP29 in the supernatant and pellet, respectively. The top gel shows the samples in the presence of 200 μM Ca^{2+}, and the bottom gel shows the samples in the presence of 2 mM EGTA.

(B) Statistical analysis for **(A)** ($n = 4$). The resulting gels were scanned to determine the distribution of actin in the supernatant: in the presence of 0, 0.4, 0.8, and 1.6 μM ABP29 and 200 μM Ca^{2+}, the percentages were 5.03, 21.75, 25.42, and 32.04%, respectively. Error bars indicate SD. Double *t* test analysis of the data shows that the percentage of actin in the supernatant in the presence of various concentrations of ABP29 and 200 μM Ca^{2+} is significantly higher than that of the control ($P < 0.05$). In the presence of 2 mM EGTA, the differences corresponding to various concentrations of ABP29 are not significant from that of the control ($P > 0.05$).

(C) Actin filaments (5 μM) labeled with Alexa 488–phalloidin were incubated with 100 nM ABP29 in the presence of 200 μM Ca^{2+}, 2 mM EGTA, or 5 μM PIP_2. Images were collected after 30 min of incubation. Double *t* test showed that there were significant differences in the length of actin filaments with 100 nM ABP29 in the presence of 200 μM Ca^{2+} (P1) compared with the control ($P1 < 0.01$) and significant differences in the length of actin filaments with 100 nM ABP29 in the presence of 2 mM EGTA (P2) or 5 μM PIP_2 (P3) compared with that in the presence of 200 μM Ca^{2+} ($P2 < 0.05$, $P3 < 0.05$). Bar = 10 μm.

(D) ABP29's severing activity is observed directly by fluorescence microscopy. Prepolymerized, Alexa 488–phalloidin-labeled actin filaments were incubated with 100 nM ABP29 in the presence of 200 μM free Ca^{2+}, and images were collected every 500 ms. Individual filaments showed an increasing number of breaks (arrowheads) as time elapsed. Bar = 10 μm.

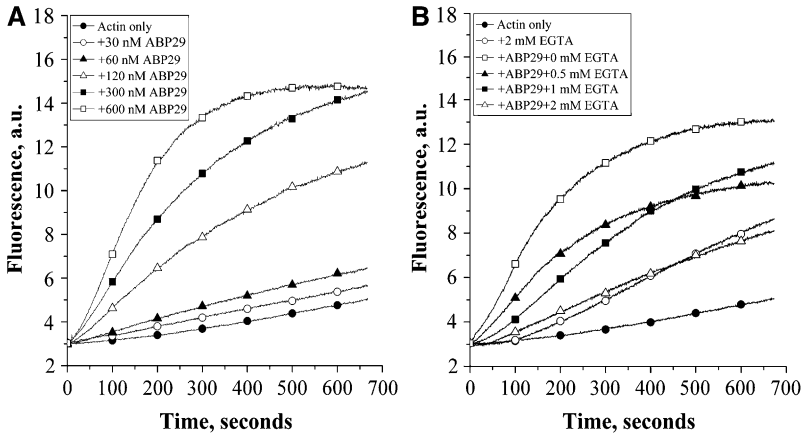

Figure 6. ABP29 Nucleates Filament Assembly from Monomers.

(A) ABP29 at various concentrations was incubated for 5 min with 5 μM actin (5% pyrene-labeled) in the presence of 200 μM free Ca^{2+}. Pyrene fluorescence (arbitrary units [a.u.]) was plotted versus time after the addition of polymerization salts to initiate polymerization.
(B) ABP29 (300 nM) was incubated for 5 min with 5 μM actin (5% pyrene-labeled) in the presence of EGTA of various concentrations. Pyrene fluorescence (arbitrary units) was plotted versus time after the addition of polymerization salts to initiate polymerization.

free Ca^{2+}. In the absence of EGTA, 300 nM ABP29 greatly shortened the lag period. With the increase in EGTA concentration, the effect of ABP29 decreased (Figure 6B). Two millimolar EGTA completely eliminated the activity of ABP29. Thus, the nucleation activity of ABP29 is regulated by Ca^{2+}.

ABP29 Caps the Barbed Ends and Inhibits Actin Filament Elongation and Depolymerization

Seed elongation assays were performed to examine the barbed end–capping activity of ABP29. One micromolar G-actin saturated with 4 μM human profilin I was added to initiate actin filament elongation at the barbed end in the presence of 200 μM free Ca^{2+}. The initial elongation rate decreased correspondingly with the substoichiometric amounts of ABP29, and 400 nM ABP29 completely suppressed the actin polymerization (Figure 7A), indicating that ABP29 could bind and cap the barbed ends of F-actin to prevent elongation from barbed ends. Similar experiments were performed in the presence of 60 nM ABP29 and various amounts of EGTA to test the Ca^{2+} dependence of the capping activity of ABP29. As shown in Figure 7B, the pyrene fluorescence increased with the increase in EGTA concentration compared with that without EGTA. Two millimolar EGTA completely abolished the ABP29 capping activity, indicating that the actin filament barbed end–capping activity of ABP29 is Ca^{2+}-dependent.

A depolymerization assay was performed to further verify the capping activity of ABP29. The experiment was performed by diluting solutions of pyrene-labeled F-actin into buffer G and monitoring the decrease in fluorescence. ABP29 at various concentrations was applied in the presence of 200 μM free Ca^{2+}. As shown in Figure 7C, 60 to 600 nM ABP29 reduced the rate of depolymerization. A low concentration of ABP29 (60 nM) inhibited the actin depolymerization effectively, and 600 nM ABP29 gave maximum inhibition. To test whether the function of ABP29 is Ca^{2+}-regulated, similar experiments were performed in the presence of 300 nM ABP29 and various amounts of EGTA. The effect of ABP29 on the actin depolymerization rate decreased with the increase in EGTA (Figure 7D), indicating that the ABP29 inhibition of actin depolymerization is regulated by Ca^{2+}. To test whether PIP_2 regulates the ABP29 capping activity, we performed depolymerization assays. Five micromolar F-actin (50% pyrene-labeled) was incubated for 5 min with 100 nM ABP29 in the presence of PIP_2 at various concentrations and 200 μM free Ca^{2+}. As shown in Figure 7E, PIP_2 by itself had no detectable effect on the actin depolymerization rate. In the presence of ABP29, however, with the increasing concentration of PIP_2, actin depolymerization became increasingly insensitive to ABP29, and 50 μM PIP_2 completely eliminated the effect of ABP29 on actin depolymerization (Figure 7E). Thus, the capping activity of ABP29 is regulated potently by PIP_2 in vitro.

ABP29 Reduces Actin Filament Length during Assembly from Monomeric Actin

Fluorescence microscopy was also applied to test the influence of ABP29 on polymerization. Five micromolar monomeric actin was polymerized for 30 min in the presence of 100 nM ABP29 and 5 μM Alexa 488–phalloidin and diluted to a final concentration of 50 nM to observe the changes in F-actin length. In the absence of ABP29, filaments per field were few and long (average mean = 12.54 ± 3.17 μm; $n = 200$) (Figure 8A), but in the presence of 100 nM ABP29, the length of actin filaments decreased sharply (average mean = 0.72 ± 0.22 μm) (Figure 8B). However, the number of filaments in the presence of ABP29 was ~10 times more than that of the control (Figures 8A and 8B). The sharp reduction in the filament lengths could be explained by the activities of ABP29 on actin nucleating, severing, and barbed end capping. Similar experiments were performed to observe whether the activity of ABP29 is regulated by Ca^{2+} and PIP_2. When 2 mM EGTA was added, the length of actin filaments was largely restored (average mean = 4.05 ± 0.96 μm) (Figure 8C), and the

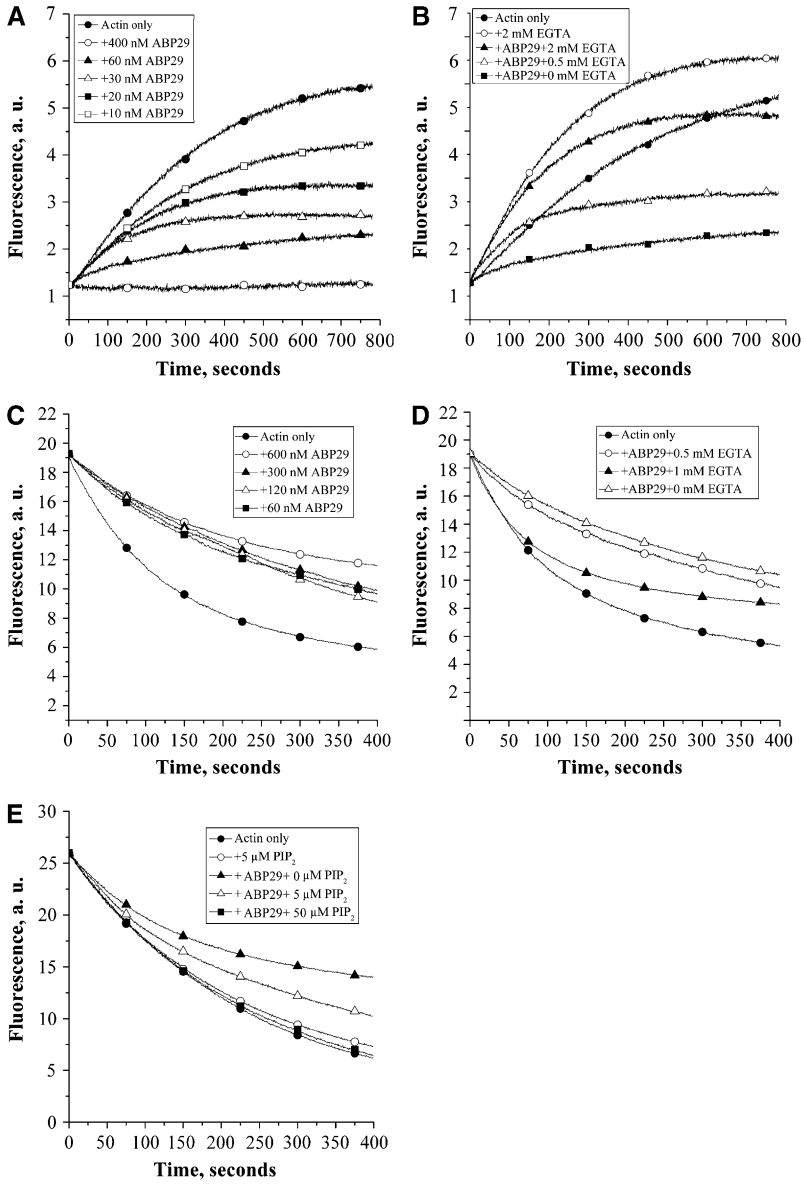

Figure 7. ABP29 Inhibits Actin Filament Elongation and Depolymerization from Barbed Ends.

(A) Preformed F-actin (0.4 μM) seeds were incubated with ABP29 at different concentrations, and 1 μM G-actin saturated with 4 μM human profilin I was added to initiate actin elongation at the barbed ends in the presence of 200 μM free Ca^{2+}.

(B) Preformed F-actin (0.4 μM) seeds were incubated with 60 nM ABP29, and 1 μM G-actin saturated with 4 μM human profilin I was added to initiate actin elongation at the barbed end in the presence of various EGTA concentrations. The change in pyrene-actin fluorescence accompanying polymerization is plotted versus time after the addition of G-actin.

(C) ABP29 at various concentrations was incubated for 5 min with 5 μM F-actin (50% pyrene-labeled) in the presence of 200 μM free Ca^{2+}.

(D) ABP29 (300 nM) was incubated for 5 min with 5 μM F-actin (50% pyrene-labeled) in the presence of EGTA of various concentrations.

(E) ABP29 (100 nM) was incubated for 5 min with 5 μM F-actin (50% pyrene-labeled) in the presence of PIP_2 of various concentrations and 200 μM free Ca^{2+}.

Pyrene fluorescence (arbitrary units [a.u.]) was plotted versus time after dilution of the solution 25-fold into buffer G.

addition of 5 μM PIP_2 led to a similar result and the average length of actin filament per field was ~6.47 ± 0.43 μm (Figure 8D), indicating that the ABP29 activity was suppressed by EGTA and PIP_2. These results further support the notion that ABP29 has Ca^{2+}- and PIP_2-regulated actin-nucleating, -severing, and barbed end–capping activity.

ABP29 Severs Actin Filaments in Plant Cells

To determine the function of ABP29 in vivo, a microinjection assay was performed using stamen hair cells from *Tradescantia fluminensis*. The central localization of the nucleus is maintained by cytoplasmic transvacuolar strands that are supported by actin

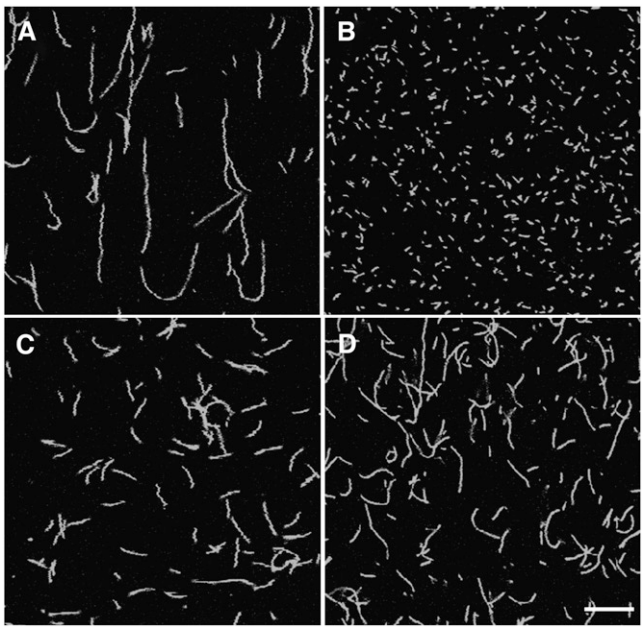

Figure 8. ABP29 Reduces Filament Length during Assembly from Monomeric Actin.

Fluorescence micrographs of individual actin filaments assembled in the presence of Ca^{2+}, EGTA, or PIP_2. In each case, 5 μM monomeric actin was polymerized for 30 min in the presence of 5 μM Alexa 488–phalloidin.
(A) Actin alone.
(B) Actin incubated with 100 nM ABP29 in the presence of 200 μM Ca^{2+}.
(C) Actin incubated with 100 nM ABP29 in the presence of 2 mM EGTA.
(D) Actin incubated with 100 nM ABP29 in the presence of 5 μM PIP_2.
Double *t* test showed that there were significant differences in the length of actin filaments with 100 nM ABP29 in the presence of 200 μM Ca^{2+} (P1) compared with the control (P1 < 0.01) and significant differences in the length of actin filaments with 100 nM ABP29 in the presence of 2 mM EGTA (P2) or 5 μM PIP_2 (P3) compared with that in the presence of 200 μM Ca^{2+} (P2 < 0.01, P3 < 0.01, respectively). Bar = 10 μm.

filament bundles. Any changes in nuclear placement are regulated by the dynamic actin organization (Gibbon et al., 1997). The effect of ABP29 on actin organization in vivo was determined by measuring the time taken for nuclear displacement. Within minutes after microinjection of ABP29, the central transvacuolar strands began to disperse and the strands became fewer and thinner, the nucleus was displaced from its original position and eventually moved to the cell cortex, and very few strands remained. The time of nuclear displacement for the cell shown in Figure 9A was ~4 min. Figure 9B shows the time for nuclear displacement calculated from the treated cells. Microinjection of buffer alone caused little nuclear displacement, resulting in the average nuclear displacement time of 13.39 ± 4.47 min ($n = 10$). ABP29 at a high concentration (60 μM) caused a dramatic increase in the rate of nuclear displacement and reduced the average time of nuclear displacement to 4.08 ± 1.07 min ($n = 18$). At lower ABP29 concentrations (30 and 15 μM), the time of nuclear displacement was 5.71 ± 1.29 min ($n = 17$) and 9.70 ± 1.81 min ($n = 13$), respectively (Figure 9B). These results indicate that ABP29 induces rapid nuclear displacement in a dose-dependent manner.

To directly observe the change in actin organization in the stamen hair cells caused by the microinjection of ABP29, Alexa 488–phalloidin (used to stain the actin filaments) was injected 5 min after the injection of ABP29. As shown in Figure 9C, the nucleus was positioned in the center of the cell and held there by the F-actin array in the control cell with microinjection of buffer alone. However, in the cell with microinjection of 60 μM ABP29, the nucleus moved toward a side wall (Figure 9D), and the central actin filament bundles were replaced by a few short and dispersed filaments (Figure 9D′). Our results confirm directly that the microinjection of ABP29 causes the disruption of central actin filament bundles.

Transient Expression of ABP29 Inhibits Lily Pollen Germination and Pollen Tube Growth and Disrupts the Actin Cytoskeleton

Microprojectile bombardment was performed to investigate the role of ABP29 in pollen germination and pollen tube growth. A pollen-specific promoter derived from *Solanum tuberosum* (Zhao et al., 2006), st901, was used to control ABP29 gene expression. The pollen germination rate and the tube growth rate transformed with green fluorescent protein (GFP) were not significantly different from those of untreated pollen (Figures 10A and 10B), indicating that the microprojectile bombardment itself or GFP had little effect on pollen germination and pollen tube growth. Moreover, as GFP fluorescence was observed at 6 h after bombardment in transformed pollen grains (Figure 10E) and pollen tubes (Figure 10F), these data showed that the st901 promoter driving the GFP expression in these experiments could be used to express ABP29.

Pollen germination and tube growth were greatly altered when transformed with ABP29. Overexpression of ABP29 decreased the pollen germination rate in a concentration-dependent manner for 4 h: the germination rate was 37% ± 5.6% ($n \geqslant 300$) when transformed with the ABP29 plasmid DNA at a lower concentration (5 μg of plasmid DNA) and 26% ± 5.3% at a higher concentration (10 μg of plasmid DNA), while the GFP-transformed control was 51% ± 9.2% (Figure 10A). Second, the length of pollen tubes growing for 4 h was shortened sharply by the overexpression of ABP29: the average length was ~84.66 ± 41 μm ($n \geqslant 100$) at a lower ABP29 concentration and 70.08 ± 33 μm at a higher ABP29 concentration, which were significantly shorter than the tubes transformed with GFP (167.15 ± 52.8 μm) (Figure 10B). There was no significant difference in the germination rates and pollen tube growth rates at 4 h compared with 6 h, indicating that expression of ABP29 exerted its greatest effect in the first 4 h (Figures 10A and 10B). Therefore, we conclude that overexpression of ABP29 prevents pollen germination and pollen tube growth.

Furthermore, the transformed pollen grains and tubes cultured for 6 h were stained with rhodamine-phalloidin in order to observe the organization of the actin cytoskeleton. The GFP-transformed pollen grains contained regular circular actin bundles, and the pollen tube contained long actin bundles in the shank and fine actin filaments in the tip region (Figures 10E′ and 10F′), which is identical to the untreated controls (Figures 10C′ and 10D′). By contrast, the pollen and pollen tubes overexpressing ABP29 contained just actin patches or short filament aggregates dispersed in the whole pollen grain and pollen tube (Figures 10G′

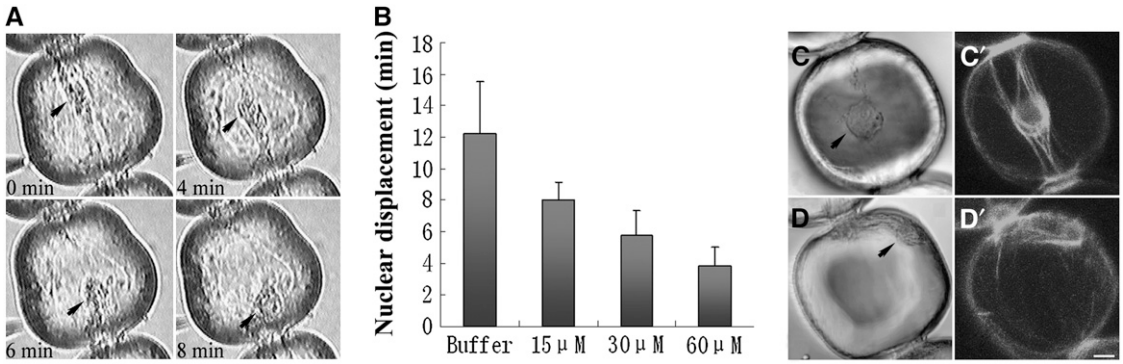

Figure 9. Microinjection of ABP29 Causes Disruption of Cytoplasmic Architecture in *Tradescantia* Stamen Hair Cells.

(A) The images were taken from the same cell at the indicated time points after microinjection with 60 μM (needle concentration) ABP29.
(B) ABP29 at different concentrations was microinjected, and the time for nuclear displacement was recorded. Columns represent the average nuclear displacement time. According to the two-tailed *t* test, the differences between the control and ABP29 at various concentrations are significant ($P < 0.05$). Error bars represent SD.
(C) and **(C′)** *Tradescantia* stamen hair cell injected with buffer alone. **(C)** shows the differential interference contrast image, and **(C′)** shows the fluorescent image labeled with Alexa 488–phalloidin.
(D) and **(D′)** *Tradescantia* stamen hair cell injected with 60 μM ABP29. **(D)** shows the differential interference contrast image, and **(D′)** shows the fluorescent image labeled with Alexa 488–phalloidin.
All images are single optical sections from the medial region. Arrowheads point to the nucleus. Bar = 10 μm.

and 10H′). However, fine actin bundles were still present in the base shank region containing lower Ca^{2+} concentration in pollen grains overexpressing ABP29. These results indicate that overexpression of ABP29 inhibits lily pollen germination and pollen tube growth by disrupting the actin cytoskeleton, probably in a Ca^{2+}-dependent manner.

In addition, transformation of pollen grains with ABP29-GFP resulted in similar effects to those seen in grains transformed with ABP29 alone (Figures 10A, 10B, 10I′, and 10J′), indicating that ABP29-GFP was biologically equivalent to ABP29 in vivo. ABP29-GFP was used to determine the localization of ABP29 in pollen grains and pollen tubes. As shown in Figure 10, there is no green fluorescence detectable in the cytoplasm of the untreated pollen (Figures 10C and 10D), but the green fluorescence in the cytoplasm of GFP- and ABP29-GFP–transformed pollen grains (Figures 10E and 10I) and the tubes (Figures 10F and 10J) was detectable at 6 h after microprojectile bombardment. The distribution of the green fluorescence in ABP29-GFP–transformed pollen tubes was similar to that of GFP-transformed pollen tubes in that there was a uniform spread of cytoplasmic fluorescence (Figures 10F and 10J). This result indicates that ABP29 is a soluble protein that localizes in the cytoplasm of pollen grains and the pollen tube, which may be responsible for the fragmentation of actin filaments.

DISCUSSION

Villin Genes Generate Novel Members of the Villin/Gelsolin/Fragmin Superfamily through Pre-mRNA Alternative Splicing in Plant Cells

The villin/gelsolin/fragmin superfamily is the only known group of Ca^{2+}-dependent actin binding proteins identified to date, which regulates a variety of cellular functions. In mammals, members of the family are encoded by separate genes and have unique functions in different kinds of cells: villin is restricted to the microvilli of brush border cells; gelsolin is expressed in a wide variety of cell types and exists as a cytoplasmic as well as a plasma isoform; CapG, the fragmin homolog in mammals, is a mediator of the endothelial cell response to mechanical forces (Pellieux et al., 2003). By contrast, bioinformatic analysis of the *Arabidopsis* and rice genomes reveals that only genes encoding the villin members are present, and separate genes encoding gelsolin/fragmin do not exist. However, several smaller members of this family, such as ABP80, ABP41, and a fragmin-like protein, were recently biochemically identified in *P. rhoeas* pollen, *L. davidii* pollen, and *M. pudica*, respectively (Yamashiro et al., 2001; Fan et al., 2004; Huang et al., 2004). Mass spectrometry revealed that all of these proteins are related to plant villin or gelsolin. These results, together with the fact that a premature stop codon is present in EST H5D9T7, which encodes *Arabidopsis* VLN1 and similar RT-PCR products and a G1-G5 protein for *Arabidopsis* VLN3, have led to the assumption that splicing variants for the villin family exist in plants (Klahre et al., 2000; Fan et al., 2004; Huang et al., 2004), although direct evidence is lacking.

Alternative splicing is an important posttranscriptional regulatory mechanism that can increase protein diversity, and recent genome-wide EST/cDNA alignments to *Arabidopsis* and rice genome databases predict that more than one-fifth of all plant genes are alternatively spliced (Wang and Brendel, 2006). Our results strongly suggest that an alternative mRNA splicing variant of *Lilium* villin (135-ABP) and its corresponding protein product are present in lily pollen. The full-length cDNA sequence encoding ABP29 was amplified from *L. longiflorum* pollen. The sequence comparison among the full-length cDNA sequence encoding ABP29, the partial genomic sequence of ABP29, and the 135-ABP

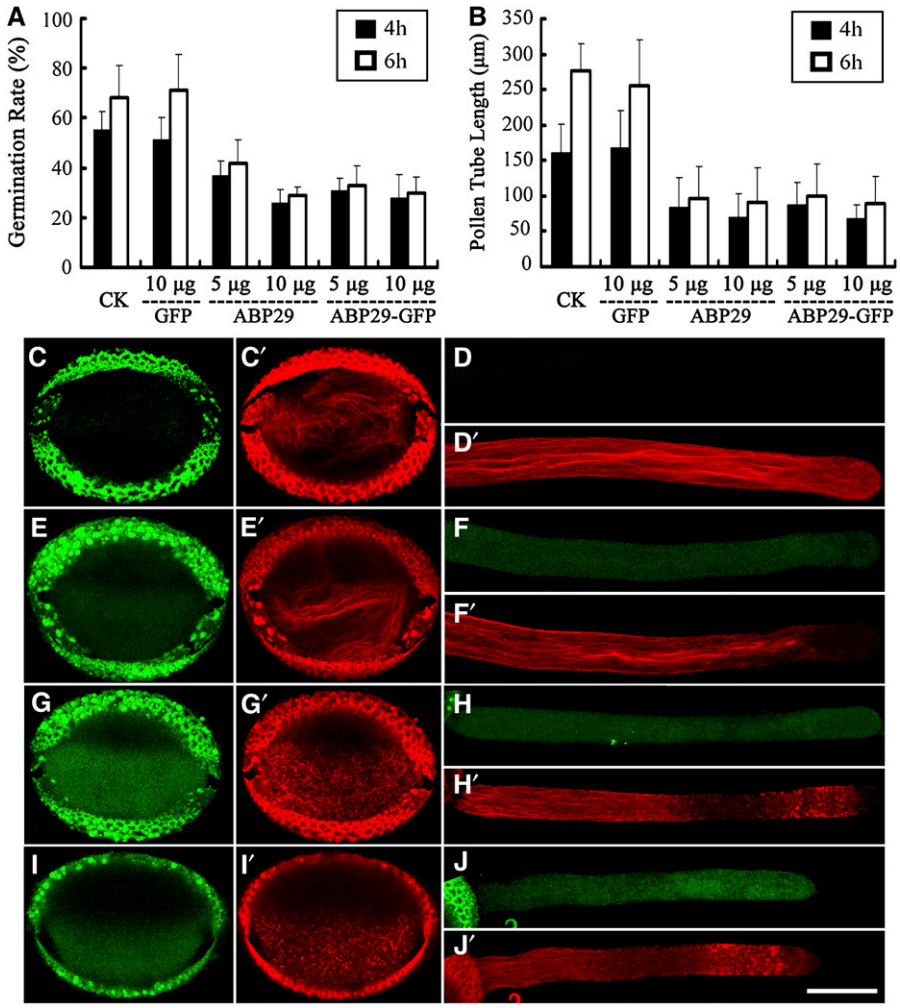

Figure 10. Transient Expression of ABP29 Suppresses Lily Pollen Tube Growth.

(A) The effect of ABP29 on pollen germination using microprojectile bombardment. After 4 h of incubation, the germination rate of pollen bombarded with the GFP-only construct showed no significant difference compared with the control untreated pollen ($P = 0.71$). There were significant differences in the germination rate of pollen bombarded with 5 and 10 μg of the ABP29 or the ABP29-GFP gene construct compared with untreated pollen or GFP-transformed pollen ($P < 0.05$). The data also showed no significant difference between ABP29-GFP– and ABP29-transformed pollen ($P < 0.05$). Error bars indicate SD. The columns represent average ratios of pollen germination, and similar results were obtained after 6 h of observation.

(B) The effect of ABP29 on pollen tube growth rate using microprojectile bombardment. After 4 h of incubation, there were no significant differences in the length of pollen tubes bombarded with GFP compared with untreated pollen tubes ($P = 0.74$). There were significant differences in the length of pollen tubes bombarded with 5 and 10 μg of ABP29 or ABP29-GFP compared with untreated pollen or GFP-transformed pollen ($P < 0.05$). The data also showed no significant difference between ABP29-GFP– and ABP29-transformed pollen ($P > 0.05$). Error bars indicate SD. The columns represent the lengths of the pollen tubes, and similar results were obtained after 6 h of observation.

(C) to **(J)** Localization of ABP29 and the effect of ABP29 on actin organization. **(C)**, **(C′)**, **(D)**, and **(D′)** show untreated pollen; **(E)**, **(E′)**, **(F)**, and **(F′)** show the GFP-only transformed pollen; **(G)**, **(G′)**, **(H)**, and **(H′)** show pollen transformed with ABP29 and GFP separately. The GFP-only construct was used as a marker for transformed pollen. **(I)**, **(I′)**, **(J)**, and **(J′)** show the ABP29-GFP transformed pollen. **(C′)** to **(J′)** are images labeled with rhodamine-phalloidin and show the in vivo actin organization, and **(C)** to **(J)** are the corresponding images, which show the intensity of the green fluorescence. The strong green or red fluorescence around the outer wall of the pollen grains is autofluorescence. These data were obtained from three independent experiments, and every condition was tested three times. Bar = 20 μm.

cDNA sequence suggests that the ABP29 transcript is an alternatively spliced product of the primary transcript of 135-ABP in which the third intron is not excised. Such a phenomenon is ascribed to a prevalent mechanism in other organisms (Kalyna et al., 2006), whereas here it is demonstrated for actin binding proteins in plant cells. The splicing mechanism of ABP29 might behave in a different manner from the other two possible splice variants reported previously. The G1-G3 splice variant for At *VLN1* results from a frameshift mutation produced by a 13-base deletion in the mRNA of At VLN1 (Klahre et al., 2000), while a

frameshift mutation caused by four extra base pairs leads to the expression of the G1-G5 protein of At VLN3 (Huang et al., 2005). We predict that the alternative splicing mechanism of ABP29 is of the alternative donor type (Wang and Brendel, 2006). To unambiguously prove this, it is important that the third intron of 135-ABP is sequenced. However, we have been unable to clone the third intron, and this is probably due to the very large size of the lily genome and excessive secondary structure. Bearing this caveat in mind, we propose that plant villin genes generate smaller members of the villin/gelsolin/fragmin superfamily and that different pre-mRNA alternative splicing mechanisms may exist to generate various members of the superfamily. This may be important in controlling the process of plant cell growth and development and deserves to be further studied.

ABP29 Containing Only the G1 and G2 Domains Functions Effectively

It is generally accepted that members of the villin/gelsolin/fragmin superfamily contain at least three gelsolin-like domains (G domains) and have evolved from a progenitor presumably containing one of these 15-kD domains (Schnuchel et al., 1995). The functions of different actin binding domains are characterized using limited proteolysis and recombinant DNA techniques. Gelsolin segment 1 (G1) is the best characterized of all domains of the gelsolin family. It was originally described as an N-terminal 17-kD chymotryptic fragment (CT14N) that retained some actin binding function (Yin et al., 1988). G1 binds actin monomers and barbed ends of actin filaments in a Ca^{2+}-independent manner. G1 with an additional 10 amino acids from the start of G2 is sufficient for weak severing activity, but the activity is ~1/100th of that presented by the whole protein. G2-G3 binds exclusively to the sides of actin filaments. Deletion analysis limited the filament binding site to G2 (Yin et al., 1988). Yu et al. (1990) showed that G1 of CapG gained the severing function when it was linked to G2-G3 of gelsolin, indicating that the F-actin side binding by G2 is a prerequisite for efficient severing. However, it is unclear whether these peptides and truncated proteins retain the conformation of the native proteins. In this study, we found that ABP29, a native protein from plants, contains only the G1 and G2 domains and a partial G2-G3 linker. Our structural model showed that G1 of ABP29 possesses conserved G-actin binding residues responsible for Ca^{2+}-dependent G-actin binding and two conserved Ca^{2+} binding F-actin binding regions in G2. In spite of a lack of the G3 domain, ABP29 administers the Ca^{2+}-dependent nucleating, severing, and capping activities in vitro. Our results show that ABP29 functions effectively in the presence of 200 μM Ca^{2+} and retains partial biochemical activity when the Ca^{2+} concentration is decreased to 40 nM. Our results indicate that G3 is not necessary for the F-actin binding, severing, and capping activities. Instead, it might function as a negative regulation domain, without which ABP29 needs less Ca^{2+} to be activated.

Severing is the process whereby noncovalent bonds between actin molecules within a filament are weakened, resulting in the filament breaking. The Ca^{2+}-free gelsolin must open at least three identifiable latches (tail latch, G1-G3 latch, and G4-G6 latch) and bind to eight calcium ions to expose the actin binding residues completely (Burtnick et al., 2004).On the contrary, ABP29 lacks G3 and latch in the predicted tertiary structure, and only three calcium ions are bound to allow binding with the actin monomer or the actin filament. Ca^{2+}-free ABP29 exists in a compact arrangement with some actin binding residues embedded in the structure. Upon binding to calcium, ABP29 was activated, exposing the actin binding surfaces on G2 and G1. The assays by fluorescence spectroscopy (Figure 5) also directly showed the Ca^{2+}-dependent severing activity of ABP29. Moreover, during the dilution- or profilin-mediated depolymerization of F-actin, severing ABPs generally function in accelerating the depolymerization of F-actin, which is usually attributed to the fact that these proteins produce additional barbed ends to promote the actin depolymerization by severing actin filaments (Huang et al., 2004; Yokota et al., 2005). However, our attention was drawn by the observation that ABP29 functions as a capping protein in inhibiting actin depolymerization, which is in contrast with the studies of Pr ABP80 using similar assays (Huang et al., 2004). This may be explained by a lack of the G3 latch in ABP29. Perhaps G1 of ABP29 can directly bind to the end of a filament through the interaction with residue Glu-167 of actin, resulting in higher capping activity. In conclusion, ABP29 containing only the G1 and G2 domains functions effectively.

Villin/Gelsolin/Fragmin Family Members Are Responsible for Several Crucial Aspects of Microfilament Structure and Organization in Pollen Tube Development

It is well known that the actin cytoskeleton is highly dynamic during the processes of pollen germination and tube growth (Vidali and Hepler, 2001). According to the spatiotemporally dynamic distribution of the actin cytoskeleton and the expression patterns of various villin/gelsolin/fragmin superfamily members found from different research groups, it can be assumed that the villin/gelsolin/fragmin superfamily plays distinctive roles in the regulation of different populations of dynamic actin cytoskeleton structure in the various phases of pollen germination and growth. It has been shown that dehydrated pollen grains contain large amounts of Ld ABP41, having a 1:10 ratio to actin and a 10:1 ratio to ABP29 (Fan et al., 2004) (see Supplemental Figure 1 online), but the amounts of Ld ABP41 decreased to one-tenth when the pollen germinated (see Supplemental Figure 1 online). Ld ABP41 has a Ca^{2+}-dependent severing function and a nucleation function (Fan et al., 2004), whereas the newly identified ABP29 acts to sever, nucleate, and cap the actin filaments. ABP29 is mainly cytoplasmic in its localization, and this is similar to other known members of the villin protein family (Yin et al., 1981; Lueck et al., 1998). However, we cannot discount the possibility that a proportion of the cyoplasmic signal is a consequence of the induced disassembly of the actin cytoskeleton. Pr ABP80, another member of the villin/gelsolin/fragmin superfamily, could also be purified from hydrated *P. rhoeas* pollen grain (Huang et al., 2004). It has a similar function to Ld ABP41 and ABP29. Therefore, they may work together to keep the form of short spicule bodies in the dehydrated pollen grain and regulate the sharply remodeled actin organization as pollen hydrates. However, 135-ABP and 115-ABP could not be detected in pollen grains (Fan et al., 2004), but they were normally purified from germinating pollen (Yokota et al., 2005). Therefore, they could

account for the formation of the stable actin bundles during the germination of pollen grains and pollen tube growth through their bundling activities (Yokota and Shimmen, 1999; Yokota et al., 2003). However, the precise spatiotemporal expression of the villin/gelsolin/fragmin superfamily members needs to be further studied in order to elucidate how they function together.

Pollen tube growth is modulated by a variety of signaling molecules. For example, the tip-focused Ca^{2+} gradient oscillates in phase with pollen tube growth (Holdaway-Clarke et al., 1997; Messerli and Robinson, 1997); Rac proteins physically interact with PtdIns P-K to synthesize PIP_2 (Kost et al., 1999); and phosphatidylinositol-specific phospholipase C (PLC) results in the hydrolysis of the membrane PIP_2 to produce the Ca^{2+}-mobilizing messenger IP_3 (Pan et al., 2005; Dowd et al., 2006). Some evidence supports the suggestion that they may act together in a common pathway to regulate polarized pollen tube growth (Kost et al., 1999; Li et al., 1999). In pollen tubes, Rop GTPase–directed polar tip growth is related to the regulation of tip-localized extracellular Ca^{2+} influxes and the formation of the intracellular tip-focused Ca^{2+} gradient in pollen tubes (Li et al., 1999). PLC-mediated IP_3 production from PIP_2 is also necessary for the Ca^{2+} gradient in pollen tubes (Franklin-Tong et al., 1996; Pan et al., 2005). For instance, the elevation of cytosolic Ca^{2+} in germinating lily pollen via calcium ionophore A23187 induced the fragmentation of actin filaments (Yokota et al., 2005). Overexpression of Rac/Rop GTPases led to the isotropic growth of pollen tubes with the formation of extensive actin cables in swollen tubes, whereas expression of dominant-negative Rac inhibited pollen tube growth via a reduction of actin bundling (Kost et al., 1999; Fu et al., 2001; Chen et al., 2003). Moreover, a catalytically inactive mutant of Pet PLC1 in pollen tubes created an expansive apical Ca^{2+} gradient in the apical region, disturbed the organization of the actin cytoskeleton, and disordered tube tip growth. As Ca^{2+}- and PIP_2-sensitive actin binding proteins, members of the villin/gelsolin/fragmin superfamily were identified in the pollen tubes and showed specific localizations and assemblies in the shank (Yokota et al., 1998) and the apex region (Fan et al., 2004; Huang et al., 2004). Experimentally, the microinjection of anti-Ld ABP41 blocked pollen tube growth (Fan et al., 2004). Furthermore, we have found that overexpression of ABP29 inhibits lily pollen germination and tube growth by disrupting the actin cytoskeleton, possibly in a Ca^{2+}-dependent manner. Therefore, it is suggested that the villin/gelsolin/fragmin superfamily is the potential downstream substrate for these signal molecules. As the sensors and regulators, the signal factors accurately regulate biochemical activities of the family members to carry out the precise dynamics of the actin cytoskeleton in pollen tube development.

METHODS

Cloning the Full-Length cDNA and Partial Genomic Sequences of ABP29

A *Lilium longiflorum* pollen expression cDNA library (kindly provided by Peter K. Hepler, University of Massachusetts) was used to isolate the full-length ABP29 cDNA by nested PCR. First, two forward primers, D1 (5′-GGGACAGAGATCTGGCGTAT-3′) and its nested oligonucleotide D2 (5′-GTTGAACTTGATGCTGTCCTTG-3′), corresponding to the 135-ABP N-terminal coding region, and the reverse primer T7 (5′-GCCCTATAGTGAGTCGTATTAC-3′) in the library vector were used to generate the 3′ end of ABP29, which was confirmed with a poly(A) tail by sequence analysis. Then, we employed the forward primer T3 (5′-ATTAACCCTACATAAAGGGA-3′) in the library vector and two specific reverse primers, U1 (5′-AGCATACAGCAGAATTAGAATTG-3′) and its nested oligonucleotide U2 (5′-TGGAATTAGCACCGTTGAATTG-3′), corresponding to the specific sequence of ABP29 in the 3′ UTR, to generate the 5′ end of ABP29. These two fragments made up a full-length cDNA and provided 3′ and 5′ end specific primers, namely the reverse primer (5′-AGTTCTTAACCATTCTTTAG-3′) and the forward primer (5′-GATCGATCCTGCGAGTCGGAAT-3′), to amplify ABP29 full-length cDNA from the pollen expression cDNA library. Total RNA from fresh *L. longiflorum* pollen was isolated using the NucleoSpin RNA plant kit (Macherey-Nagel) to further confirm the above result, and RT-PCR resulted in the identical sequence using the same conditions and primers. The partial genomic sequence for ABP29 was amplified from the genomic DNA of *L. longiflorum* with the forward primer (5′-GTTGAACTTGATGCTGTCCTTG-3′) and the reverse primer (5′-CTCATTTTCTATATTTTATGTTC-3′), corresponding to the identical sequence of ABP29 and 135-ABP cDNA and the specific sequence of ABP29, respectively.

Plasmid Construction

An *Eco*RI site and an *Xba*I site were introduced at the 5′ end of the ABP29 coding region, and an *Xho*I site was introduced at the 3′ end, by PCR. For *Escherichia coli* expression, the A-tailed amplified product was cloned into the pGEM-T vector to create the plasmid pGEM-ABP29, which was digested with *Eco*RI and *Xho*I and ligated into pGEX-4T vector (Amersham) restricted with the same enzymes to produce the plasmid pGEX-4T-ABP29. For pollen expression, the *Xba*I-*Sac*I fragment from pGEX-4T-ABP29 was cloned into the pCAMBIA1300 vector (Amersham), introducing a pollen-specific promoter, st901, to construct the binary vector pCAMBIA1300-st901-ABP29. For ABP29 localization, a C-terminal fusion of ABP29 with GFP was also constructed by PCR-based methodology, introducing a *Sac*I site at the 3′ end of the GFP coding region. The A-tailed amplified product was cloned into the pGEM-T vector to create the plasmid pGEM-ABP29-GFP. The *Xba*I-*Sac*I fragment from this was cloned into pCAMBIA1300-st901 vector to create the plasmid pCAMBIA1300-st901-ABP29-GFP. The pCAMBIA1300-st901-GFP construct was generated for the analysis of st901 promoter activity in lily pollen and the pCAMBIA1300-st901-GUS construct for supplementation up to a consistent amount of total plasmid DNA in each sample. All sequences of the cloned cDNAs were confirmed by sequence analysis.

Expression and Purification of Recombinant ABP29

The pGEX-4T-ABP29 construct was transformed into strain BL21 (DE3) of *E. coli*. The cells were grown to an OD_{600} of 0.8 at 37°C and then induced with the addition of 0.4 mM isopropyl-D-thiogalactopyranoside at 26°C overnight. Cells were collected by centrifugation and resuspended in PBS (137 mM NaCl, 2.7 mM KCl, 10 mM Na_2HPO_4, and 2 mM KH_2PO_4, pH 8.0) supplemented with 0.5 mM phenylmethylsulfonyl fluoride (PMSF), 10 mg/mL aprotinin, 10 mg/mL leupeptin, and 10 mg/mL pepstatin. After sonication and centrifugation (23,000*g*, 30 min), the supernatant was incubated with glutathione–Sepharose 4B resin (Novagen), washed with PBS, and eluted with elution buffer (20 mM Tris-HCl, pH 8.0, and 10 mM reduced glutathione). The purified recombinant ABP29 was dialyzed against buffer A3 (2 mM Tris-HCl, 0.2 mM $CaCl_2$, 0.2 mM ATP, and 0.2 mM DTT, pH 8.0).

Actin Nucleation Assay

Actin was isolated from rabbit skeletal muscle acetone powder with the method described by Pardee and Spudich (1982) and was labeled on

Cys-374 with pyrene iodoacetamide according to the method of Pollard (1983). Actin nucleation was essentially performed according to Huang et al. (2004). Five micromolar G-actin (5% pyrene-labeled) was incubated for 5 min at room temperature with ABP29 at different concentrations in the presence of 200 μM free Ca^{2+} or with 300 nM ABP29 in the presence of EGTA of various concentrations. Pyrene fluorescence was monitored for 400 s after the supplementation of one-tenth volume of 10×F buffer (buffer A3 with the addition of 500 mM KCl, 25 mM $MgCl_2$, and 2.5 mM ATP). Free Ca^{2+} in the presence of EGTA was calculated with winmaxc32 software by Petesmif (P. M. Smith, University of Liverpool), which is available at http://www.stanford.edu/~cpatton/maxc.html. According to our calculation, 2 mM EGTA was equivalent to the volume of 40.5 nM free [Ca^{2+}], 1 mM EGTA equal to 91.1 nM [Ca^{2+}], and 0.5 mM EGTA equal to 243 nM [Ca^{2+}] in all of our experiment systems. This experiment and the following functional assays were all repeated independently at least three times using separate new preparations of each sample.

High-Speed Cosedimentation Assays

A high-speed cosedimentation assay was used to determine ABP29's F-actin binding and severing activities in the presence of free Ca^{2+} at various concentrations. All proteins were centrifuged at 200,000*g* for 1 h before use. In a 200-μL reaction volume, ABP29 at different concentrations was mixed with 5 μM preformed F-actin (50 mM KCl, 5 mM $MgCl_2$, and 0.5 mM ATP were added to the 5 μM G-actin sample and incubated at 4°C for 16 h) in the presence of 200 μM free Ca^{2+} or 2 mM EGTA at 22°C for 1 h. In addition, F-actin without ABP29 was used as the control. The samples were centrifuged at 200,000*g* for 1 h in a TLA-110 rotor (Beckman) at 4°C. Equal amounts of pellet and supernatant samples were separated by 12% SDS-PAGE. The gels were stained with Coomassie Brilliant Blue R 250.

Elongation Assay to Determine the Capping Activity of ABP29 for the F-Actin Barbed End

After 0.4 μM preformed F-actin seeds was incubated with ABP29 at different concentrations at room temperature for 5 min, 1 μM G-actin saturated with 4 μM human profilin I and one-tenth volume of 10×F buffer were added to initiate actin elongation at the barbed end of actin filaments in the presence of 200 μM free Ca^{2+}. To test whether the affinity of ABP29 was Ca^{2+}-dependent, preformed F-actin (0.4 μM) seeds were incubated with 60 nM ABP29 in the presence of EGTA of various concentrations, and 1 μM G-actin saturated with 4 μM human profilin I was added as above. The change in pyrene fluorescence accompanying actin polymerization was monitored after the actin elongation was initiated.

Dynamics of Actin Filament Depolymerization

Five micromolar preformed F-actin (50% pyrene-labeled) was incubated with ABP29 of various concentrations at room temperature for 5 min in the presence of 200 μM free Ca^{2+}, and the solution was diluted 25-fold into buffer G (2 mM Tris-HCl, 0.2 mM $CaCl_2$, 0.2 mM ATP, and 0.2 mM DTT, pH 8.0) at room temperature. To further observe whether the effect of ABP29 on the dynamics of actin filament depolymerization is Ca^{2+}-dependent, 5 μM F-actin (50% pyrene-labeled) was incubated for 5 min with 300 nM ABP29 in the presence of EGTA of different concentrations, and the solution was diluted as given above. The change in pyrene fluorescence accompanying actin depolymerization was monitored for 400 s after dilution.

To test the effect of phospholipids on ABP29's capping activity, a depolymerization assay was performed in the presence of PIP_2 (Sigma-Aldrich) micelles of varying concentrations. Experimental conditions for measuring the changes in F-actin levels were as described above, except that ABP29 was preincubated with PIP_2 at different amounts for 5 min on ice before the addition of preformed pyrene-actin.

Fluorescence Microscope Visualization of Actin Filaments

In the experiment to visualize the effect of ABP29 on the generation of actin filaments during nucleation, 5 μM G-actin together with 100 nM ABP29 in the presence of 200 μM free Ca^{2+} or 2 mM EGTA was polymerized in 1×F buffer at room temperature for 30 min and labeled with an equimolar amount of Alexa 488–phalloidin (Molecular Probes) during polymerization. In the experiment to test ABP29's severing activity, 5 μM prepolymerized actin filaments labeled with an equimolar amount of Alexa 488–phalloidin was incubated with 100 nM ABP29 in the presence of 200 μM free Ca^{2+} or 2 mM EGTA at room temperature for 30 min or observed directly by fluorescence microscopy. All of the polymerized F-actin was diluted to 50 nM, and the diluted sample of 2 μL was added to a 22 × 22-mm cover slip coated with poly-Lys (0.01%) before observation. Actin filaments for static observation were viewed using a confocal laser scanning microscope (Olympus FV-300) mounted on an inverted microscope (Olympus IX-70) using a ×60 oil-immersion objective, and the images were collected by Olympus Fluoview 4.0 software. In the dynamic observation, actin filaments were viewed with a microscope (Carl Zeiss 200M) equipped with a ×63 1.5 numerical aperture Planapo objective, and digital images were collected with an Axio CamMR charge-coupled device camera using Axiovision software.

Purification of Ca^{2+}-Dependent Actin Binding Proteins from Dehydrated Lily Pollen

The method for isolating Ca^{2+}-dependent actin binding proteins from lily pollen was performed as described by Fan et al. (2004) with some modifications. Ten grams of *Lilium davidii* pollen grains in 50 mL of extraction buffer (0.1 M Tris, 0.4 M sorbitol, 32 mg/mL polyvinylpyrrolidone-10, 0.5 mM $CaCl_2$, 50 mM NaF, 10% glycerol, 0.5 mM ATP, 5 mM DTT, 0.5 mM PMSF, 10 mg/mL aprotinin, 10 mg/mL leupeptin, and 10 mg/mL pepstatin, pH 8.0) was ground in a mortar for 30 min on ice and centrifuged at 100,000*g* for 60 min at 4°C. The supernatant was loaded onto the DNase I affinity column preequilibrated with the extraction buffer and then washed with 15 column volumes of Ca^{2+} buffer (0.1 M Tris-HCl, 0.5 mM $CaCl_2$, 10% glycerol, 0.5 mM ATP, 5 mM DTT, 0.5 mM PMSF, 10 mg/mL aprotinin, 10 mg/mL leupeptin, and 10 mg/mL pepstatin, pH 7.5). Finally, 20 mL of the EGTA buffer (0.1 M Tris, 0.5 mM EGTA, 0.5 mM ATP, 5 mM DTT, 10 mg/mL aprotinin, 10 mg/mL leupeptin, and 10 mg/mL pepstatin, pH 7.5) was used to elute Ca^{2+}-sensitive actin binding proteins from the affinity column. Protein concentration was measured using the Bradford reagent (Bio-Rad Laboratories), and BSA was the standard.

To prepare the pollen total protein samples for immunoblotting, 1 g each of dehydrated pollen, hydrated pollen, and germinated pollen was suspended in 3 mL of extraction buffer (50 mM Tris-HCl, pH 7.4, 10% sucrose, 10 mM Na_3VO_4, 10 mM NaF, 1 mM tartrate, 1 mM PMSF, 5 μg/mL leupeptin, and 5 μg/mL antipain) and ground on ice for 5 min. After centrifugation two times at 15,000 rpm for 30 min at 4°C, the supernatant was dissolved using 5× SDS sample loading buffer and boiled for 5 min.

Immunoblotting

Purification of the Ld ABP41 antibody was performed as described by Fan et al. (2004). After SDS-PAGE, proteins on the 12% polyacrylamide gel were electrophoretically transferred to a polyvinylidene difluoride membrane (Millipore) according to the method of Towbin et al. (1992), and the sheet was blocked with Tris-buffered saline (10 mM Tris-HCl, pH 7.4, and 150 mM NaCl) containing 5% BSA and 0.5% Tween 20 for 90 min. Purified Ld ABP41 polyclonal antibody was diluted 100-fold with Tris-buffered saline supplemented with 2% BSA and 0.1% Tween 20. Anti-rabbit IgG conjugated with alkaline phosphatase was diluted 5000-fold as secondary antibody.

Microinjection

Stamen hairs were collected from open flowers of *Tradescantia fluminensis* for microinjection as described previously (Staiger et al., 1994; Karakesisoglou et al., 1996; Jing et al., 2003). The microinjection system (model IM-16; Narishige Instrument) was attached to a light microscope (Leica model DMLFS). The images were obtained with a video camera (JVC CK-C138EG), and the whole process was recorded with a tape recorder. ABP29 was prepared by exchanging the extraction buffer with an injection buffer (10 mM Tris-HCl, 0.2 mM $CaCl_2$, 0.2 mM ATP, and 0.5 mM DTT, pH 7.0). The in vivo effects of the proteins were compared by monitoring their disruptive effect on the actin-dependent position of the nucleus. Time 0 was marked when the entire contents of the injection needle entered the cytoplasm, and each cell was monitored for a maximum of 20 min. Displacement of the nucleus was measured by monitoring how soon the nucleus moved completely outside the perimeter defined by its edge at time 0. At least 10 successful injections of each sample were used for the statistical analysis, as well as four kinds of agents: injection buffer and ABP29 of 15, 30, and 60 μM were injected into live stamen hair cells. F-actin in live stamen hair cells was stained by microinjection of 20 μM Alexa 488–phalloidin, and images were acquired with a confocal laser scanning microscope (Olympus FV300-IX70). Cells were imaged through a ×60 Olympus Planapo objective; the fluorescent probes were excited using the 488-nm line of the argon laser. Optical sections in 0.5 μm steps were collected and projected with Fluoview 4.0 software.

Particle Bombardment–Mediated Transient Expression in Lily Pollen

Transient transformation of lily pollen by microprojectile bombardment was used to study the influence exerted by the overexpression of ABP29 on lily pollen tube growth. Frozen *L. davidii* pollen grains (stored at −20°C after dehydration) were hydrated overnight at 4°C. A total of 0.02 g of lipid-removed pollen grains was suspended in 40 μL of pollen germination medium (GM; containing 15% sucrose, 1.6 mM H_3BO_3, 1 mM KCl, and 0.1 mM $CaCl_2$, pH 5.6, adjusted with MES or Tris) and then spotted onto a 10-mm layer made of 20 μL of 1% GM-prepared low melting temperature agarose (agarose type VII; Sigma-Aldrich) in a 34-mm Petri dish.

As a control, gold particles (2.4 mg per sample) were coated with 10 μg of plasmid pCAMBIA1300-st901-GFP and used to analyze the st901 activity (Figures 10E and 10F). In another four bombardments, 5 and 10 μg of plasmid pCAMBIA1300-st901-ABP29 were combined with 5 μg of pCAMBIA1300-st901-GFP (as a marker of transformed pollen) and used for pollen growth–related measurements (Figures 10G and 10H), and 5 and 10 μg of plasmid pCAMBIA1300-st901-ABP29-GFP were used to coat gold particles for the ABP29 localization (Figures 10I and 10J). In each of the five samples, the amount of total plasmid DNA was increased to 15 μg by the supplementation of pCAMBIA1300-st901-GUS, to ensure that comparable amounts of DNA were transformed into the bombarded pollen grains. Preformed microprojectiles were dripped over a macrocarrier, and three microprojectile bombardments per sample were started using a PDS-1000/He particle delivery system (Bio-Rad Laboratories). During bombardment, the microcarrier launch assembly was placed in the first slot from the top (level 1), and lily pollen grains were placed at level 3, so that the distance from the stopping screen to the target cells was 8 cm. We employed rupture discs of 1100 p.s.i. to accelerate macrocarriers under a 27-inch mercury vacuum. Lily pollen grains mixed with GM were washed from the agarose layer by 1.3 mL of GM added to the Petri dish immediately after bombardment. The transformed pollen grains in random visual fields of each sample were photographed for growth-related calculation at specific times after the initiation of culturing on a rotary shaker at 16°C. The transformed pollen grains with newly emerging tubes >10 μm long were scored to measure the germinating percentage. The pollen tubes showing green fluorescence were photographed to measure pollen tube length.

Labeling of Microfilaments in Pollen Grains and Tubes

A modified method from Wang et al. (2005) was used in this experiment. The germinated pollen was fixed with vacuum-infiltration for the first 5 min in fixation buffer (4% paraformaldehyde, 50 mM PIPES, and 10% sucrose, pH 6.9) and then kept in the fixation medium for 1 h. After fixation, the germinated pollen was washed three times in 50 mM PIPES buffer, pH 6.9, and then incubated for 1 h in the dark with 60 nM rhodamine-phalloidin (Molecular Probes) in buffer (50 mM PIPES, 10% sucrose, 1% DMSO, and 0.01% Nonidet P-40, pH 6.9). The stained pollen grains and tubes were transferred into a flow chamber on a slide and visualized with an inverted microscope equipped with a confocal laser scanning microscope (Olympus FV300-IX 70). The fluorescent probes were excited using the 488-nm (green) and 543-nm (red) lines of the argon laser. Optical sections in 0.6- to 0.8-μm steps were collected and projected with Fluoview 4.0 software. Images were further processed with Adobe Photoshop 7.0.

Accession Numbers

Sequence data from this article can be found in the GenBank/EMBL data libraries under the following accession numbers: ABP29 (EF042093), partial genomic sequence of ABP29 (EF042092), G1-G5 protein for At VLN3 (AY093052), 135-ABP (AAD54660), At villin1 (NP_029567), At villin2 (NP_565958), At villin3 (NP_567048), and At villin4 (AAO64915).

Supplemental Data

The following material is available in the online version of this article.

Supplemental Figure 1. Dynamic Expression of Villin/Gelsolin/Fragmin Superfamily Proteins at Different Stages during the Pollen-Germinating Process.

ACKNOWLEDGMENTS

We thank Jianmin Zhou (National Institute of Biological Science, Beijing, China) and Bo Liu (University of California at Davis) for detailed discussions and suggestions. We thank Peter K. Hepler (University of Massachusetts) for kindly providing us with the lily pollen cDNA expression library and Jingjuan Yu (China Agricultural University) for kindly providing us with the st901 promoter. We also thank Chengcai Chu (Chinese Academy of Sciences) for supplying the microprojectile bombardment instrument and Chuanmao Zhang (Peking University) for helping with living image microscopy. This work was supported by awards from the National Natural Science Foundation of China (Grants 30630005, 30470176, and 30325005) and the National Basic Research Program of China (Grant 2006CB100100) to H.R.

Received October 23, 2006; revised May 14, 2007; accepted June 4, 2007; published June 22, 2007.

REFERENCES

Burtnick, L.D., Koepf, E.K., Grimes, J., Jones, E.Y., Stuart, D.I., McLaughlin, P.J., and Robinson, R.C. (1997). The crystal structure of plasma gelsolin: Implications for actin severing, capping, and nucleation. Cell **90:** 661–670.

Burtnick, L.D., Urosev, D., Irobi, E., Narayan, K., and Robinson, R.C. (2004). Structure of the N-terminal half of gelsolin bound to actin: Roles in severing, apoptosis and FAF. EMBO J. **23:** 2713–2722.

Chen, C.Y.-h., Cheung, A.Y., and Wu, H.-m. (2003). Actin-depolymerizing factor mediates Rac/Rop GTPase-regulated pollen tube growth. Plant Cell **15:** 237–249.

Choe, H., Burtnick, L.D., Mejillano, M., Yin, H.L., Robinson, R.C., and Choe, S. (2002). The calcium activation of gelsolin: Insights from the 3A structure of the G4–G6/actin complex. J. Mol. Biol. **324:** 691–702.

Dowd, P.E., Coursol, S., Skirpan, A.L., Kao, T.H., and Gilroy, S. (2006). *Petunia* phospholipase c1 is involved in pollen tube growth. Plant Cell **18:** 1438–1453.

Fan, X., Hou, J., Chen, X., Chaudhry, F., Staiger, C.J., and Ren, H. (2004). Identification and characterization of a Ca^{2+}-dependent actin filament-severing protein from lily pollen. Plant Physiol. **136:** 3979–3989.

Franklin-Tong, V.E. (1999). Signaling and the modulation of pollen tube growth. Plant Cell **11:** 727–738.

Franklin-Tong, V.E., Drobak, B.K., Allan, A.C., Watkins, P., and Trewavas, A.J. (1996). Growth of pollen tubes of *Papaver rhoeas* is regulated by a slow-moving calcium wave propagated by inositol 1,4,5-trisphosphate. Plant Cell **8:** 1305–1321.

Friederich, E., Pringault, E., Arpin, M., and Louvard, D. (1990). From the structure to the function of villin, an actin-binding protein of the brush border. Bioessays **12:** 403–408.

Fu, Y., Wu, G., and Yang, Z. (2001). Rop GTPase-dependent dynamics of tip-localized F-actin controls tip growth in pollen tubes. J. Cell Biol. **152:** 1019–1032.

Furuhashi, K., and Hatano, S. (1989). A fragmin-like protein from plasmodium of *Physarum polycephalum* that severs F-actin and caps the barbed end of F-actin in a Ca^{2+}-sensitive way. J. Biochem. (Tokyo) **106:** 311–318.

Gibbon, B.C., Ren, H., and Staiger, C.J. (1997). Characterization of maize (*Zea mays*) pollen profilin function *in vitro* and in live cells. Biochem. J. **327:** 909–915.

Hartwig, J.H., and Kwiatkowski, D.J. (1991). Actin-binding proteins. Curr. Opin. Cell Biol. **3:** 87–97.

Hepler, P.K., Vidali, L., and Cheung, A.Y. (2001). Polarized cell growth in higher plants. Annu. Rev. Cell Dev. Biol. **17:** 159–187.

Holdaway-Clarke, T.L., Feijo, J.A., Hackett, G.R., Kunkel, J.G., and Hepler, P.K. (1997). Pollen tube growth and the intracellular cytosolic calcium gradient oscillate in phase while extracellular calcium influx is delayed. Plant Cell **9:** 1999–2010.

Huang, S., Blanchoin, L., Chaudhry, F., Franklin-Tong, V.E., and Staiger, C.J. (2004). A gelsolin-like protein from *Papaver rhoeas* pollen (PrABP80) stimulates calcium-regulated severing and depolymerization of actin filaments. J. Biol. Chem. **279:** 23364–23375.

Huang, S., Robinson, R.C., Gao, L.Y., Matsumoto, T., Brunet, A., Blanchoin, L., and Staiger, C.J. (2005). *Arabidopsis* VILLIN1 generates actin filament cables that are resistant to depolymerization. Plant Cell **17:** 486–501.

Hussey, P.J., Ketelaar, T., and Deeks, M.J. (2006). Control of the actin cytoskeleton in plant cell growth. Annu. Rev. Plant Biol. **57:** 109–125.

Jing, Y.P., Yi, K.X., and Ren, H.Y. (2003). Actins from plant and animal sources tend not to form heteropolymers *in vitro* and function differently in plant cells. Protoplasma **222:** 183–191.

Kalyna, M., Lopato, S., Voronin, V., and Barta, A. (2006). Evolutionary conservation and regulation of particular alternative splicing events in plant SR proteins. Nucleic Acids Res. **34:** 4395–4405.

Karakesisoglou, I., Schleicher, M., Gibbon, B.C., and Staiger, C.J. (1996). Plant profilins rescue the aberrant phenotype of profilin-deficient *Dictyostelium* cells. Cell Motil. Cytoskeleton **34:** 36–47.

Klahre, U., Friederich, E., Kost, B., Louvard, D., and Chua, N.H. (2000). Villin-like actin-binding proteins are expressed ubiquitously in Arabidopsis. Plant Physiol. **122:** 35–48.

Kost, B., Lemichez, E., Spielhofer, P., Hong, Y., Tolias, K., Carpenter, C., and Chua, N.H. (1999). Rac homologues and compartmentalized phosphatidylinositol 4,5-bisphosphate act in a common pathway to regulate polar pollen tube growth. J. Cell Biol. **145:** 317–330.

Li, H., Lin, Y., Heath, R.M., Zhu, M.X., and Yang, Z. (1999). Control of pollen tube tip growth by a Rop GTPase-dependent pathway that leads to tip-localized calcium influx. Plant Cell **11:** 1731–1742.

Lueck, A., Brown, D., and Kwiatkowski, D.J. (1998). The actin-binding proteins adseverin and gelsolin are both highly expressed but differentially localized in kidney and intestine. J. Cell Sci. **111:** 3633–3643.

Messerli, M., and Robinson, K.R. (1997). Tip localized Ca^{2+} pulses are coincident with peak pulsatile growth rates in pollen tubes of *Lilium longiflorum.* J. Cell Sci. **110:** 1269–1278.

Monteiro, D., Liu, Q., Lisboa, S., Scherer, G.E., Quader, H., and Malho, R. (2005). Phosphoinositides and phosphatidic acid regulate pollen tube growth and reorientation through modulation of $[Ca^{2+}]_c$ and membrane secretion. J. Exp. Bot. **56:** 1665–1674.

Nakayasu, T., Yokota, E., and Shimmen, T. (1998). Purification of an actin-binding protein composed of 115-kDa polypeptide from pollen tubes of lily. Biochem. Biophys. Res. Commun. **249:** 61–65.

Pan, Y.Y., Wang, X., Ma, L.G., and Sun, D.Y. (2005). Characterization of phosphatidylinositol-specific phospholipase C (PI-PLC) from *Lilium davidii* pollen. Plant Cell Physiol. **46:** 1657–1665.

Pardee, J.D., and Spudich, J.A. (1982). Purification of muscle actin. Methods Cell Biol. **24:** 271–289.

Pellieux, C., Desgeorges, A., Pigeon, C.H., Chambaz, C., Yin, H., Hayoz, D., and Silacci, P. (2003). Cap G, a gelsolin family protein modulating protective effects of unidirectional shear stress. J. Biol. Chem. **278:** 29136–29144.

Pollard, T.D. (1983). Measurement of rate constants for actin filament elongation in solution. Anal. Biochem. **134:** 406–412.

Robinson, R.C., Mejillano, M., Le, V.P., Burtnick, L.D., Yin, H.L., and Choe, S. (1999). Domain movement in gelsolin: A calcium-activated switch. Science **286:** 1939–1942.

Schnuchel, A., Wiltscheck, R., Eichinger, L., Schleicher, M., and Holak, T.A. (1995). Structure of severin domain 2 in solution. J. Mol. Biol. **247:** 21–27.

Staiger, C.J., and Hussey, P.J. (2004). Actin and actin-modulating proteins. In The Plant Cytoskeleton in Cell Differentiation and Development, P.J. Hussey, ed (Oxford, UK: Blackwell Publishers), pp. 32–80.

Staiger, C.J., Yuan, M., Valenta, R., Shaw, P.J., Warn, R.M., and Lloyd, C.W. (1994). Microinjected profilin affects cytoplasmic streaming in plant cells by rapidly depolymerizing actin microfilaments. Curr. Biol. **4:** 215–219.

Sun, H.Q., Yamamoto, M., Mejillano, M., and Yin, H.L. (1999). Gelsolin, a multifunctional actin regulatory protein. J. Biol. Chem. **274:** 33179–33182.

Tao, Z., and Ren, H. (2003). Regulation of gelsolin to plant actin filaments and its distribution on pollen. Sci. China C Life Sci. **46:** 379–388.

Tominaga, M., Yokota, E., Vidali, L., Sonobe, S., Hepler, P.K., and Shimmen, T. (2000). The role of plant villin in the organization of the actin cytoskeleton, cytoplasmic streaming and the architecture of the transvacuolar strand in root hair cells of *Hydrocharis.* Planta **210:** 836–843.

Towbin, H., Staehelin, T., and Gordon, J. (1992). Electrophoretic transfer of proteins from polyacrylamide gels to nitrocellulose sheets: Procedure and some applications. 1979. Biotechnology **24:** 145–149.

Vandekerckhove, J. (1990). Actin-binding proteins. Curr. Opin. Cell Biol. **2:** 41–50.

Vidali, L., and Hepler, P.K. (2001). Actin and pollen tube growth. Protoplasma **215:** 64–76.

Vidali, L., Yokota, E., Cheung, A.Y., Shimmen, T., and Hepler, P.K. (1999). The 135 kDa actin-bundling protein from *Lilium longiflorum* pollen is the plant homologue of villin. Protoplasma **209:** 283–291.

Wang, B.B., and Brendel, V. (2006). Genomewide comparative analysis of alternative splicing in plants. Proc. Natl. Acad. Sci. USA **103:** 7175–7180.

Wang, L., Liu, Y.M., and Li, Y. (2005). Comparison of F-actin fluorescent labeling methods in pollen tubes of *Lilium davidii.* Plant Cell Rep. **24:** 266–270.

Wu, W., and Yan, L.F. (1997). Identification of gelsolin by western blotting in maize pollen. Chin. Sci. Bull. **42:** 1784–1786.

Yamamoto, K., Pardee, J.D., Reidler, J., Stryer, L., and Spudich, J.A. (1982). Mechanism of interaction of *Dictyostelium severin* with actin filaments. J. Cell Biol. **95:** 711–719.

Yamashiro, S., Kameyama, K., Kanzawa, N., Tamiya, T., Mabuchi, I., and Tsuchiya, T. (2001). The gelsolin/fragmin family protein identified in the higher plant *Mimosa pudica.* J. Biochem. (Tokyo) **130:** 243–249.

Yin, H.L., Albrecht, J.H., and Fattoum, A. (1981). Identification of gelsolin, a Ca^{2+}-dependent regulatory protein of actin gel-sol transformation, and its intracellular distribution in a variety of cells and tissues. J. Cell Sci. **91:** 901–906.

Yin, H.L., Iida, K., and Janmey, P.A. (1988). Identification of a polyphosphoinositide-modulated domain in gelsolin which binds to the sides of actin filaments. J. Cell Biol. **106:** 805–812.

Yokota, E., and Shimmen, T. (1999). The 135-kDa actin-bundling protein from lily pollen tubes arranges F-actin into bundles with uniform polarity. Planta **209:** 264–266.

Yokota, E., Takahara, K.-i., and Shimmen, T. (1998). Actin-bundling protein isolated from pollen tubes of lily. Biochemical and immunocytochemical characterization. Plant Physiol. **116:** 1421–1429.

Yokota, E., Tominaga, M., Mabuchi, I., Tsuji, Y., Staiger, C.J., Oiwa, K., and Shimmen, T. (2005). Plant villin, lily P-135-ABP, possesses G-actin binding activity and accelerates the polymerization and depolymerization of actin in a Ca^{2+}-sensitive manner. Plant Cell Physiol. **46:** 1690–1703.

Yokota, E., Vidali, L., Tominaga, M., Tahara, H., Orii, H., Morizane, Y., Hepler, P.K., and Shimmen, T. (2003). Plant 115-kDa actin-filament bundling protein, P-115-ABP, is a homologue of plant villin and is widely distributed in cells. Plant Cell Physiol. **44:** 1088–1099.

Yu, F.X., Johnston, P.A., Sudhof, T.C., and Yin, H.L. (1990). gCap39, a calcium ion- and polyphosphoinositide-regulated actin capping protein. Science **250:** 1413–1415.

Yu, F.X., Sun, H.Q., Janmeyg, P.A., and Yin, H.L. (1992). Identification of a polyphosphoinositide-binding sequence in an actin monomer-binding domain of gelsolin. J. Biol. Chem. **267:** 14616–14621.

Zhao, Y., Zhao, Q., Ao, G., and Yu, J. (2006). Characterization and functional analysis of a pollen-specific gene st901 in *Solanum tuberosum.* Planta **224:** 405–412.